SANDIA REPORT

SAND2021-11991
Printed September 2021

Sandia National Laboratories

3D orthorhombic earth model effects on seismic source characterization

Richard P. Jensen, Leiph A. Preston

Prepared by
Sandia National Laboratories
Albuquerque, New Mexico 87185
Livermore, California 94550

Issued by Sandia National Laboratories, operated for the United States Department of Energy by National Technology & Engineering Solutions of Sandia, LLC.

Available to DOE and DOE contractors from

U.S. Department of Energy
Office of Scientific and Technical Information
P.O. Box 62
Oak Ridge, TN 37831

Telephone: (865) 576-8401
Facsimile: (865) 576-5728
E-Mail: reports@osti.gov
Online ordering: http://www.osti.gov/scitech

Available to the public from

U.S. Department of Commerce
National Technical Information Service
5301 Shawnee Road
Alexandria, VA 22312

Telephone: (800) 553-6847
Facsimile: (703) 605-6900
E-Mail: orders@ntis.gov
Online order: https://classic.ntis.gov/help/order-methods

3D orthorhombic earth model effects on seismic source characterization

Richard P. Jensen, Ph.D.
Geomechanics Department

Leiph A. Preston, Ph.D.
Geophysics Department

Sandia National Laboratories
P.O. Box 5800
Albuquerque, NM 87185-0671

.

SAND2021-11991

ABSTRACT

Most earth materials are anisotropic with regard to seismic wave-speeds, especially materials such as shales, or where oriented fractures are present. However, the base assumption for many numerical simulations is to treat earth materials as isotropic media. This is done for simplicity, the apparent weakness of anisotropy in the far field, and the lack of well-characterized anisotropic material properties for input into numerical simulations. One approach for addressing the higher complexity of actual geologic regions is to model the material as an orthorhombic medium. We have developed an explicit time-domain, finite-difference (FD) algorithm for simulating three-dimensional (3D) elastic wave propagation in a heterogeneous orthorhombic medium.

The objective of this research is to investigate the errors and biases that result from modeling a non-isotropic medium as an isotropic medium. This is done by computing "observed data" by using synthetic, anisotropic simulations with the assumption of an orthorhombic, anisotropic earth model. Green's functions for an assumed isotropic earth model are computed and then used an inversion designed to estimate moment tensors with the "observed" data. One specific area of interest is how shear waves, which are introduced in an anisotropic model even for an isotropic explosion, affect the characterization of seismic sources when isotropic earth assumptions are made. This work is done in support of the modeling component of the Source Physics Experiment (SPE), a series of underground chemical explosions at the Nevada National Security Site (NNSS).

ACKNOWLEDGMENT

The Source Physics Experiment (SPE) would not have been possible without the support of many people from several organizations. The authors wish to express their gratitude to theNational Nuclear Security Administration (NNSA), Defense Nuclear Nonproliferation Research and Development (DNN R&D), and SPE working group, a multi-institutional and interdisciplinary group of scientists and engineers. Appreciation is also extended to Christian Poppeliers for his assistance with the inversion and for his thorough review of this work.

CONTENTS

LIST OF FIGURES

LIST OF TABLES

NOMENCLATURE

3D	three-dimensional
CMPL	convolutional perfectly matched layer
DNN R&D	Defense Nuclear Nonproliferation Research and Development
FD	finite-difference
GF	Green's Function
Hz	Hertz
m	meter
MPI	message passing interface
MPML	multi-axial perfectly matched layer
MRF	moment rate function
NNSA	National Nuclear Security Administration
NNSS	Nevada National Security Site
PDE	partial differential equation
PML	perfectly matched layer
SPE	Source Physics Experiment
STF	source time function

1. INTRODUCTION

At the micro scale, the earth comprises a wide variety of minerals, which, as a function of its crystalline structure, gives rise to seismic anisotropy. This anisotropy manifests as varying seismic wave speeds as a function of the direction of propagation. At a larger, or macro, scale, features such as oriented fractures and layered structures give rise to seismic anisotropy in the bulk earth. However, often, the randomness of mineral orientation in rocks, at the large scale, can be viewed as a quasi-isotropic medium, where much of the seismic anisotropy present in the individual mineral constituents becomes averaged. Additionally, at a large enough scale, the oriented fractures and geologic structures average to a nearly isotropic, or at most, a weakly anisotropic medium. Thus, it is not uncommon to assume the earth is approximately an isotropic medium, especially since the solution of the isotropic wave equations are much less computationally demanding compared to the equations describing wave propagation in an anisotropic medium.

However, there are instances where solutions of the anisotropic wave equations are necessary. Shales are well-known to be strongly anisotropic due to their finely layered structure and preferred mineral orientations (e.g., Johnston and Christensen, 1995 [5]). Additionally, smaller scale studies where fractures or fabrics are strongly oriented in a region will necessitate the use of anisotropy. For example, the upper mantle under oceanic crust exhibits anisotropy due to tectonic flow causing olivine crystals to form in a preferential direction (e.g., Hess, 1964 [4]). There are some locations where seismic anisotropy is required to model the structure at-large, even to first order accuracy. However, as computational resources continue to expand, the ability to model areas of weak anisotropy will produce more accurate simulations, allowing a deeper understanding of the earth itself and the processes that produce and propagate seismic waves through the earth.

Characterizing geologic media as a dense system of vertically aligned microfractures superimposed on a finely-layered horizontal geology typical of shallow crustal rocks lends itself to being modeled as an orthorhombic elastic medium. Orthorhombic anisotropy is a special form of general anisotropy characterized by three orthogonal symmetry planes (Tsvankin, 1991 [13]). This reduces the number of elastic moduli from 21 in a general anisotropic medium to 9. Physically, this can be represented as oriented vertical fractures or fabric superimposed on a horizontally layered structure (Schoenberg and Helbig, 1997 [12]).

By assuming three mutually orthogonal symmetry planes, these moduli can be determined by observing (or prescribing) nine independent P-wave and S-wave speeds along different propagation directions. Preston (2018) [11] developed an explicit time-domain finite-difference (FD) algorithm for simulating 3D elastic wave propagation in a heterogeneous orthorhombic medium. The components of the particle velocity vector and the stress tensor are governed by a set of nine, coupled, first-order, linear, partial differential equations (PDEs) called the velocity-stress system. All time and space derivatives are discretized with centered and staggered FD operators possessing second- and fourth-order temporal and spatial numerical accuracy, respectively. Additionally, we have implemented a novel perfectly matched layer (PML) absorbing boundary conditions, specifically designed for orthorhombic media, to effectively suppress grid boundary reflections.

Pararhombi is a newly developed massively parallelized 3D full waveform simulation algorithm for use in orthorhombic media within its principal coordinate system. This restriction allows the equations to be discretized and solved in the same manner as an isotropic media — only the elastic moduli are different. Thus, Pararhombi retains much of the computational efficiency of isotropic solutions but, at the same time, providing higher accuracy in real world applications. The basic theory behind full waveform simulation in orthorhombic media and the implementation is detailed in Preston (2018 [11]).

The objective of this research is to investigate the errors and biases that result from modeling a non-isotropic medium as an isotropic medium. This is done by computing "observed data" by using synthetic, anisotropic simulations with the assumption of an orthorhombic, anisotropic earth model. Green's functions for an assumed isotropic earth model are computed and then used in moment tensor inversion with the "observed" data. One specific area of interest is how shear waves, which are introduced in an anisotropic model even for an isotropic explosion, affect the characterization of seismic sources when isotropic earth assumptions are made. This work is done in support of the modeling component of the SPE, a series of underground chemical explosions at the NNSS.

2. PARARHOMBI THEORY AND IMPLEMENTATION

The theory and implementation of Pararhombi, which is a parallel implementation of 3D seismic wave propagation code for orthorhombic media, is briefly outlined in this section. A complete treatment of the theory, implementation, and validation can be found in Preston, 2018 [11].

2.1. Theory

The basic physical theory of seismic propagation within an orthorhombic media is well known and is outlined in this section for completeness. We will start with general anisotropy in a linear elastic media and then specialize to orthorhombic anisotropy. The equations of motion and the constitutive equations, which describe the relationship between stress and strain, are (e.g., Aki and Richards, 2002 [1]):

$$\frac{\partial v_i(\mathbf{x},t)}{\partial t} = \frac{1}{\rho(\mathbf{x})}\left(\frac{\partial \sigma_{ij}(\mathbf{x},t)}{\partial x_j} + f_i(\mathbf{x},t)\right) \tag{1}$$

$$\frac{\partial \sigma_{ij}(\mathbf{x},t)}{\partial t} = C_{ijkl}(\mathbf{x})\frac{\partial v_k(\mathbf{x},t)}{\partial x_l} + \frac{\partial m_{ij}(\mathbf{x},t)}{\partial t} \tag{2}$$

where v_i is the i^{th} component of particle velocity, σ_{ij} is a component of the 3x3 symmetric stress tensor, ρ is density, f_i is a body force source term, C_{ijkl} is the elastic modulus tensor, m_{ij} is a symmetric moment tensor source, $\mathbf{x}$ is a point in (assumed) 3-D space, and t is time. In Equations 1 and 2 repeated indices imply summation (Einstein summation convention). C_{ijkl} is a 4^{th} rank tensor; thus, it has 81 elements. However, it can be shown through symmetries of the stress and strain tensors and energy considerations that only 21 of these elements can be independent in a general anisotropic media (Aki and Richards, 2002 [1]). Equation 1 expresses the equations of motion, whereas Equation 2 is the time derivative of the stress-strain constitutive equations. Because of the of symmetries in C_{ijkl} mentioned above, one can write the stress-strain relationship in a more compact form often referred to as Voigt notation (e.g., Musgrave, 1970 [8]).

2.1.1. Orthorhombic Media

An orthorhombic media is characterized by three mutually orthogonal planes of symmetry (Figure 2-1 a))(Tsvankin, 1991 [13]). This symmetry reduces the number of independent elastic moduli from 21 to 9. Physically, an orthorhombic media can arise intrinsically from the crystal structure of minerals. However, often in seismology the media of interest is a macroscopic assemblage of minerals with randomized orientations such that much of the intrinsic anisotropy is nullified for long wavelengths and a quasi-isotropic material results. Orthorhombic media can also arise structurally with a common example being vertical fractures within a layered media (Figures 2-1 a) and b))(Tsvankin, 1991 [13]; Schoenberg and Helbig, 1997 [12]). This is not due to any particular mineral constituents, but due to the macroscopic interplay of the various

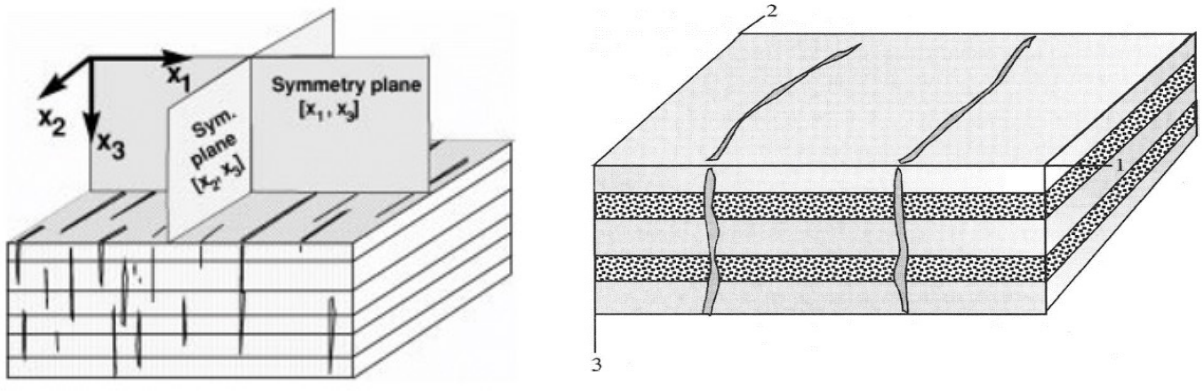

Figure 2-1 (a) Symmetry planes in an orthorhombic geologic medium (from Tsvankin, 1991). (b) Example orthorhombic media formed by a superposition of vertical fractures within a layered medium (from Schoenberg and Helbig, 1997).

geological layers and fractures that produces orthorhombic seismic wave propagation for wavelengths with respect to the layer thickness and fracture density.

In an orthorhombic media, the 21 independent elements of C_{ijkl} in Equation 1 can be simplified, reduced to nine elements and written in Voigt notation for the coordinate system where the symmetry planes coincide with the principal coordinate planes to:

$$\begin{bmatrix} \sigma_{xx} \\ \sigma_{yy} \\ \sigma_{zz} \\ \sigma_{yz} \\ \sigma_{xz} \\ \sigma_{xy} \end{bmatrix} = \begin{bmatrix} C_{xxxx} & C_{xxyy} & C_{xxzz} & 0 & 0 & 0 \\ C_{xxyy} & C_{yyyy} & C_{yyzz} & 0 & 0 & 0 \\ C_{xxzz} & C_{yyzz} & C_{zzzz} & 0 & 0 & 0 \\ 0 & 0 & 0 & C_{yzyz} & 0 & 0 \\ 0 & 0 & 0 & 0 & C_{xzxz} & 0 \\ 0 & 0 & 0 & 0 & 0 & C_{xyxy} \end{bmatrix} \begin{bmatrix} \varepsilon_{xx} \\ \varepsilon_{yy} \\ \varepsilon_{zz} \\ \varepsilon_{yz} \\ \varepsilon_{xz} \\ \varepsilon_{xy} \end{bmatrix} \tag{3}$$

Note there are now nine independent components as required by an orthorhombic system. Of course, any rotation of the system out of the principal coordinates will generally fill in the remainder of the elements in matrix C_{ijkl}. By restricting the formulation to the special case where we are in the principal coordinate system, we can use the special properties of Equation 3 to build a simplified system of equations for Pararhombi. A detailed explanation and formulation of the system of equations can be found in the verification documentation of Pararhombi (Preston, 2018 [11]).

2.1.2. Moduli-Wave Speed Conversions

Often the elastic moduli in geologic media are not directly known; however, seismic wave speeds may be known or estimated along several different directions of wave propagation. From this wave speed information, one can compute the necessary moduli. Cheadle et al. (1991) [3] provides the necessary equations to perform the conversions from wave speed to moduli. One must know the P- and S-wave speeds for propagation along each of the principal coordinate

directions (six wave speeds), plus either P-wave or S-wave speeds at a 45° angle within each of the principal coordinate planes (three more wave speeds). Assuming that P-wave speeds are measured at a 45° angle within each plane, Table 2-1 shows the elastic modulus tensor components, where V_{Px} is the P-wave speed along the x-axis; V_{Sxy} is the S-wave speed for propagation along the x-axis, polarized in the y-direction, or vice-versa; V_{Pxy} is the P-wave speed for propagation in the x-y plane at 45° from the axes; other symbols are similarly denoted.

Table 2-1 Elastic modulus tensor components.

$C_{xxxx} = \rho V_{Px}^2$	$C_{yzyz} = \rho V_{Syz}^2$	$C_{xxyy} = \rho \left[\sqrt{\left(2V_{Pxy}^2 - V_{Px}^2 - V_{Sxy}^2\right)\left(2V_{Pxy}^2 - V_{Py}^2 - V_{Sxy}^2\right)} - V_{Sx}^2 \right]$
$C_{yyyy} = \rho V_{Py}^2$	$C_{xzxz} = \rho V_{Sxz}^2$	$C_{xxzz} = \rho \left[\sqrt{\left(2V_{Pxz}^2 - V_{Px}^2 - V_{Sxz}^2\right)\left(2V_{Pxz}^2 - V_{Pz}^2 - V_{Sxz}^2\right)} - V_{Sx}^2 \right]$
$C_{zzzz} = \rho V_{Pz}^2$	$C_{xyxy} = \rho V_{Sxy}^2$	$C_{yyzz} = \rho \left[\sqrt{\left(2V_{Pyz}^2 - V_{Pz}^2 - V_{Syz}^2\right)\left(2V_{Pyz}^2 - V_{Py}^2 - V_{Syz}^2\right)} - V_{Sx}^2 \right]$

2.1.3. Physical Constraints on the Wave Speeds

The basic physical and mathematical constraint on the moduli (or wave speeds) derives from the fact that the matrix C_{ijkl} in Equation 3 must be positive definite. This is a broad constraint that in many circumstances can be difficult to analytically impose for general problems. Wave speeds and densities must be real and positive; thus, equations in the first two columns of Table 2-1 immediately imply their respective moduli must be real, positive numbers. This also follows from the necessary condition that the matrix C_{ijkl} in Equation 3 be positive definite. Equations in the first two columns of Table 2-1 are the diagonal elements of that matrix. Physically, all the elastic moduli must be real numbers as well. This places some constraints on the relationship among the wave speeds in order to keep C_{xxyy}, C_{xxzz}, and C_{yyzz} real. These equations imply the constraints shown in Table 2-2.

Note that with these constraints, the moduli given by C_{xxyy}, C_{xxzz}, and C_{yyzz} can be negative. Since these are off-diagonal elements of the matrix in Equation 3 , this is allowable, but physically unusual (Schoenberg and Helbig, 1997 [12]). The above conditions impose primarily the mathematical constraint that the system be positive definite. This is a necessary condition for physicality, but there may be additional physical constraints beyond the mathematical ones that are not fully understood for an orthorhombic media. In isotropic media, positive definiteness simply requires $V_S < V_P$; however, geophysically we often assume that $V_S < 2V_P/\sqrt{3}$. This latter condition keeps the bulk modulus positive, whereas the former would allow a negative bulk

modulus. Schoengerg and Helbig (1997) [12] choose to impose some additional constraints on the orthorhombic system to keep the system more geologically reasonable. They require that the minimum P-wave speed over all directions be larger than the maximum S-wave speed over all directions. This is analogous to the isotropic positive definiteness requirement.

Table 2-2 Constraints on relationship of wave speeds.

$V_{Pxy} \geq \sqrt{\frac{1}{2}\left(2V_{Px}^2 + V_{Sxy}^2\right)}$	$V_{Pxz} \geq \sqrt{\frac{1}{2}\left(2V_{Px}^2 + V_{Sxz}^2\right)}$	$V_{Pyz} \geq \sqrt{\frac{1}{2}\left(2V_{Py}^2 + V_{Syz}^2\right)}$
$V_{Pxy} \geq \sqrt{\frac{1}{2}\left(2V_{Py}^2 + V_{Sxy}^2\right)}$	$V_{Pxz} \geq \sqrt{\frac{1}{2}\left(2V_{Pz}^2 + V_{Sxz}^2\right)}$	$V_{Pyz} \geq \sqrt{\frac{1}{2}\left(2V_{Pz}^2 + V_{Syz}^2\right)}$

2.1.4. Stress-Free Surface Condition

At the earth's surface, the air above the earth could be modeled as an isotropic fluid (zero shear moduli) with appropriate bulk modulus. However, another alternative is to approximate the surface of the earth as a stress-free boundary condition. From a seismological perspective, air is shear-free and has a bulk modulus that is orders of magnitude smaller than rock; thus, it can be considered non-existent — a vacuum. At an interface between two elastic materials, the normal components of the stresses must be continuous across the boundary (Aki and Richards, 2002 [1]). Since a vacuum can support zero shear or compressive stresses, the stress components normal to the surface must be zero at the earth's surface in this approximation. The implementation of this boundary condition can be seen in (Preston, 2018 [11]).

2.2. Code Implementation

The structure of the matrix C_{ijkl} in Equation 3 is identical to that of an isotropic medium; only the relationship among the moduli is different and are as follows: $C_{xxxx} = C_{yyyy} = C_{zzzz} = \lambda + 2\mu$, $C_{xxyy} = C_{xxzz} = C_{yyzz} = \lambda$, and $C_{xyxy} = C_{xzxz} = C_{yzyz} = \mu$ for an isotropic medium, where λ and μ are the Lamé parameters. Thus, numerical techniques used for isotropic elastic media can also be used in the principal coordinate system for orthorhombic media.

2.2.1. Finite Difference Grid

The computer code, Pararhombi, uses a standard staggered finite-difference scheme (Virieux, 1986 [14]) to discretize the coupled, first-order system of partial differential equations given by

Equations 1 and 2. In this scheme all time and space derivatives can be computed using centered finite-difference operators. The 3D model space is discretized into cells of equal sizes, with the corners of each cell containing compressive stress nodes, the centers of the edges of each cell containing particle velocity nodes, and the centers of faces corresponding to shear stress nodes (Figure 2-2). Compressive stress moduli and densities are coincident with compressive stress nodes (dependent variables) and shear moduli are located coincidentally with shear stress dependent variables. Densities are interpolated onto velocity dependent variable positions using 2^{nd} order interpolation. Thus, compressive stress nodes, moduli, and all densities are located at integer index locations; velocities are located at half-integer locations in its corresponding component direction (e.g., v_x is located at a half-integer location in x, but integer location in y and z); and shear stresses and moduli are located at half-integer locations for the two coordinates corresponding to its component (e.g., σ_{xy} is located at half-integer locations for x and y, but at an integer location for z). Temporally, both compressive and shear stresses are updated at integer time steps. All three velocity components are updated on half-integer time steps.

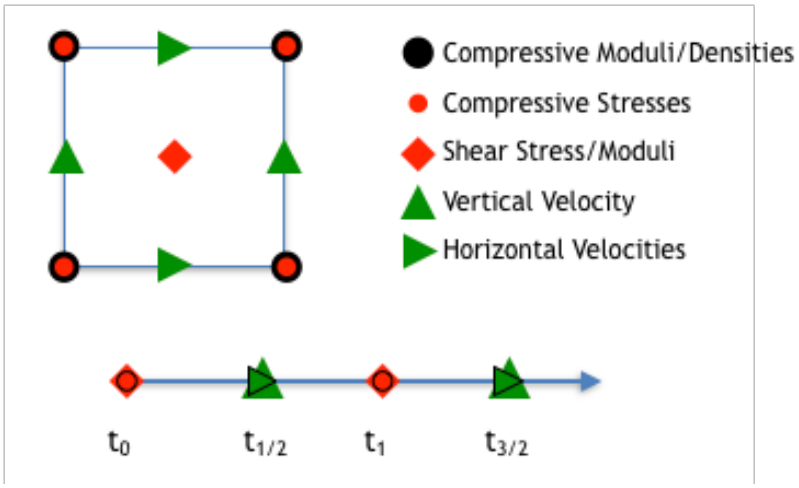

Figure 2-2 One face of a unit-cell (top) and time axis (bottom) for the staggered finite-difference scheme.

2.2.2. Finite Difference Equations

The partial differential equations given by Equations 1 and 2 are discretized according to the grid outlined in Section 2.2.1 and solved using 4^{th} and 2^{nd} order accurate finite-difference operators in space and time, respectively. Standard Taylor Series finite-difference coefficients are used by default, but others may be substituted if desired. Pararhombi utilizes an explicit, leap-frog approach for time stepping.

2.2.3. Absorbing Boundary Conditions

Often it is desired to only run a simulation of a portion of the earth, instead of the whole earth. When one truncates the earth model at artificial boundaries defined by the numerical 3D domain of the simulation space, it produces artificial reflections at these boundaries that are unphysical. In

order that the solution not be polluted by these artificial reflections, an absorbing boundary is constructed along the flanks of the model space to mitigate these undesirable artifacts. Pararhombi uses a multi-axial perfectly matched layer (MPML) (Meza-Fajardo and Papageorgiou, 2008 [7]) to efficiently absorb the numerical domain boundary reflections. MPMLs are similar to classical PMLs (Berenger, 1994 [2]) and convolutional perfectly matched layers (CMPLs) (Komatitsch and Martin, 2007 [6]).

2.2.4. Massively Parallel Implementation

Pararhombi uses the message passing interface (MPI) to divide the problem into smaller portions that multiple cores and/or machines can work on simultaneously. The full 3D model domain is subdivided into user-specified subdomains that allow parallel computation. Only nodes directly on the edges of each of these subdomains need to share information with their direct neighbors. This allows high parallel efficiency in optimal circumstances.

3. SIMULATION MODELS

There are two basic models that were used for the simulations.

3.1. Model One

The first model is essentially a quarter symmetry model that has a model extent in the positive X, Y, and Z directions and a reduced extent in the negative X, Y, and Z directions that is only large enough to accommodate an absorbing boundary. The model extent, the location of the receiver lines, and the location of the source can be seen in Figure 3-1. The model has a grid that is 551 x 551 x 551 (X, Y, Z, respectively) and grid points at a 2-meter (m) grid spacing. The boundary at Z=-100 m (assumed to be the surface of the earth) is modeled as a stress-free boundary. When the wave speeds are assumed to be isotropic, all the boundaries are a 40m thick CMPL except the free surface. For the model using anisotropic wave speeds, all the boundaries are a 40m thick MPML with a 5% cross-factor on all boundaries, except the free surface. The source is located at X = Y = Z = 0 m. There are seven receiver lines with 18 receivers per line. The location, length, and orientation can be seen in Figure 3-1 and are detailed in Table 3-1.

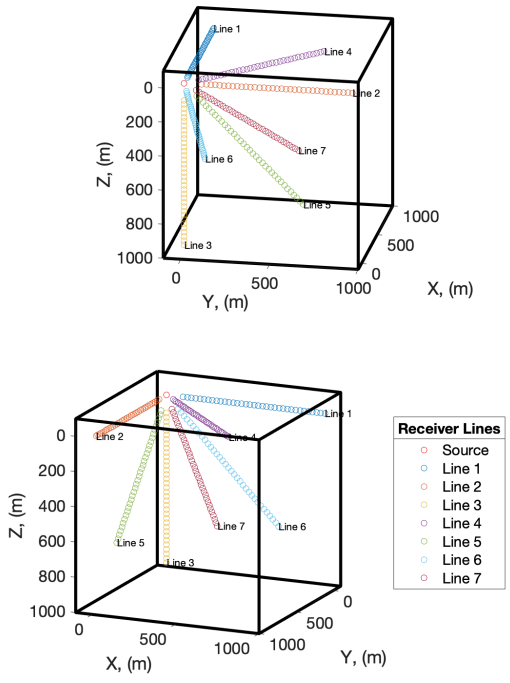

Figure 3-1 First model showing the model extent, the location of the receiver lines, and the location of the source.

Table 3-1 Receiver line locations.

Line 1	along X-axis; $Y = Z = 0$
Line 2	along Y-axis; $X = Z = 0$
Line 3	along Z-axis; $X = Y = 0$
Line 4	$X = Y; Z = 0$
Line 5	$X = 0; Y = Z$
Line 6	$X = Z; Y = 0$
Line 7	$X = Y = Z$

3.2. Model Two

The second model has an equal extent in both the positive X and Y directions. The boundary at Z=0 (assumed to be the surface of the earth) is modelled as a stress-free boundary. The model extent, the location of the receiver lines, and the location of the source can be seen in Figure 3-2. The model has a grid that is 1001 x 1001 x 503 (X, Y, Z, respectively) grid points at a 2-m grid spacing. The boundary at Z = 0 m (assumed to be the surface of the earth) is modeled as a stress-free boundary. When the wave speeds are assumed to be isotropic, all the boundaries are a 40-m thick CMPL except the free surface. For the model using anisotropic wave speeds, all the boundaries are a 40-m thick MPML with a 5% cross-factor on all boundaries, except the free surface. The source is located at X =0 m, Y = 0 m, and Z = 100 m. There are eight receiver lines with 18 receivers per line at a depth of Z = 1 m. The location, length, and orientation can be seen in Figure 3-2 and are detailed in Table 3-2.

Table 3-2 Receiver line locations. All receivers are at $z = 0$ m

.

	Azimuth
Line 1	90°
Line 2	45°
Line 3	0°
Line 4	300°
Line 5	270°
Line 6	205°
Line 7	180°
Line 8	110°

3.3. Reference Source Time Function

"Observed data" is created by convolving the Green's Functions (GFs) (resulting from simulations of the anisotropic model with different sources—these will be defined) with a source

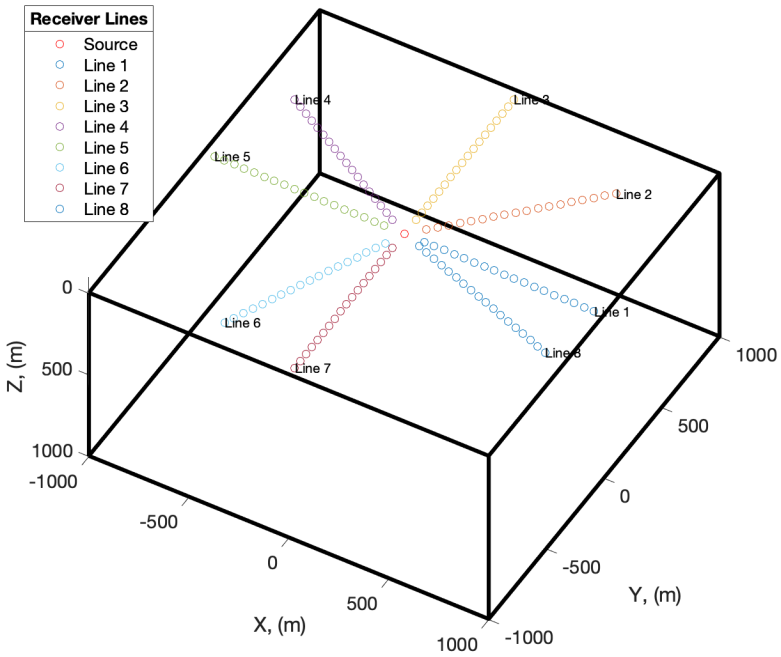

Figure 3-2 Second model showing the model extent, the location of the receiver lines, and the location of the source.

time function (STF). The same reference STF used for creating the "observed data", is used consistently for all simulations. The reference STF used is an Error Function with a mode frequency of 30 Hertz (Hz). For easier comparison with results shown in Chapter 4, Figure 3-3(B) shows the moment rate function (MRF), i.e. the time derivative of the STF . Figure 3-3(A) shows the shape of the curve of the STF used in creating all "observed data".

3.4. Isotropic model source functions

Three source types were simulated in isotropic models to use in the inversion for the STF with the "observed data": 1) Isotropic explosion source, 2) Non-isotropic explosion moment tensor source (M_{XX}, M_{YY}, and M_{ZZ}) and 3) General moment tensor source (M_{XX}, M_{YY}, M_{ZZ}, M_{XY}, M_{XZ}, and M_{YZ}).

3.5. Isotropic model parameters

The material parameters for the isotropic models, both Model One and Model Two, are identical. They are as follows:

- $V_p = 3500 m/s$

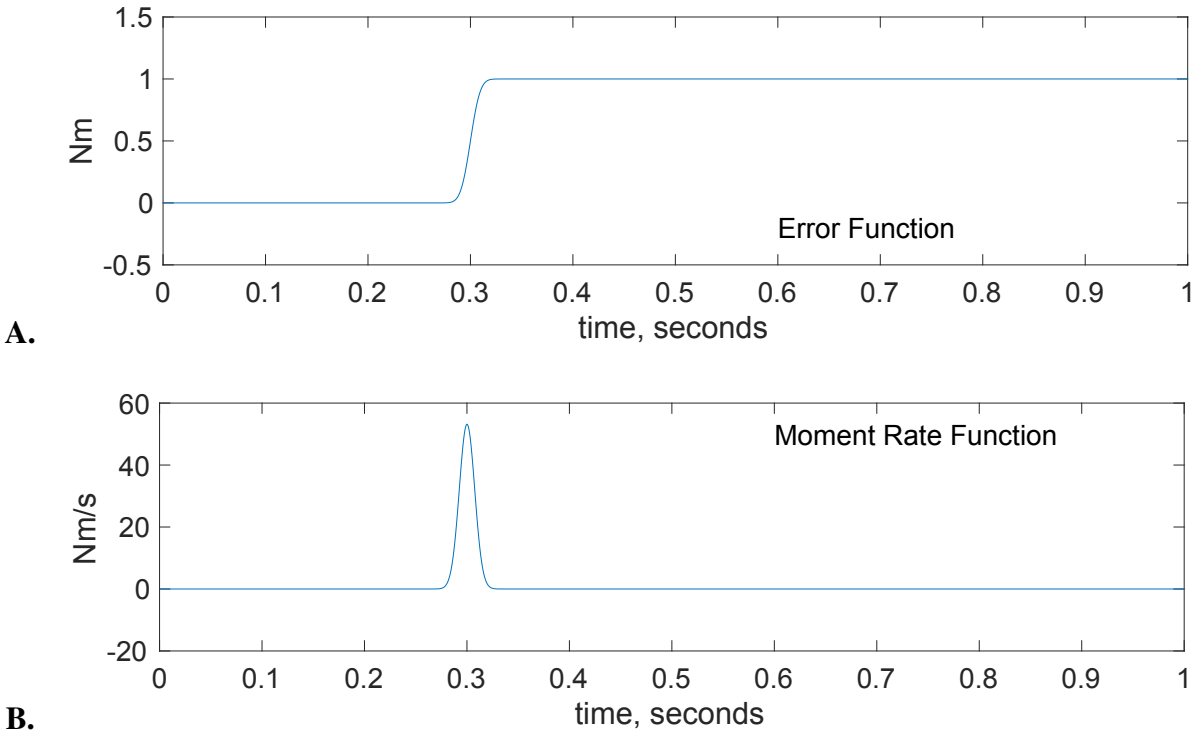

Figure 3-3 A.) Error Function, or source time function (STF). B.) Time derivative of the error function, or moment rate function (MRF)

- $V_s = 1565 m/s$
- $\rho = 1930 kg/m^3$

Where V_p is the compressional (P) wave-speed, V_s is the shear (S) wave-speed, and ρ is the density.

3.6. Creation of "observed data"

Sets of "observed data" were created for Model One (see Section 3.1) and for Model Two (see Section 3.2). Pararhombi models, which were based on anisotropic material parameters, were used to compute GFs. The computed GFs were then convolved with the Source Time Function (see Section 3.3)

3.6.1. Model One "observed data" material parameters

There are two different sets of anisotropic model parameters. The only difference between the two sets is in the P wave-speeds in the Y- and Z- directions (V_{py} and V_{pz}). Table 3-3 shows the difference between the two models. The differing data sets are designated as 1-1 and 1-2, where

the first number indicates the model number and the second number indicates the material parameter set.

Table 3-3 Material parameters for Model One anisotropic sets. Highlighted rows indicate the difference between the two models. The differing data sets are designated as 1-1 and 1-2.

	1st Anisotropic Model 1-1	2nd Anisotropic Model 1-2
V_{Pxx}	3850 m/s	3850 m/s
V_{Pyy}	3150 m/s	3850 m/s
V_{Pzz}	3500 m/s	3150 m/s
V_{Pxy}	3500 m/s	3500 m/s
V_{Pxz}	3500 m/s	3500 m/s
V_{Pyz}	3500 m/s	3500 m/s
V_{Sxy}	1565 m/s	1565 m/s
V_{Sxz}	1565 m/s	1565 m/s
V_{Syz}	1565 m/s	1565 m/s
ρ	1930 kg/m^3	1930 kg/m^3

3.6.2. Model Two "observed data" material parameters

For the Model Two "observed data", we used three different sets of material parameters. The values are shown in Table 3-4.

Table 3-4 Material parameters for Model Two anisotropic sets. The differing data sets are designated as 2-1, 2-2, and 2-3

	1st Anisotropic Model 2-1	2nd Anisotropic Model 2-2	2nd Anisotropic Model 2-3
V_{Pxx}	3850 m/s	3570 m/s	3850 m/s
V_{Pyy}	3150 m/s	3430 m/s	3150 m/s
V_{Pzz}	3500 m/s	3500 m/s	3500 m/s
V_{Pxy}	3500 m/s	3520 m/s	3600 m/s
V_{Pxz}	3500 m/s	3535 m/s	3675 m/s
V_{Pyz}	3500 m/s	3465 m/s	3325 m/s
V_{Sxy}	1565 m/s	1642 m/s	1950 m/s
V_{Sxz}	1565 m/s	1487 m/s	1175 m/s
V_{Syz}	1565 m/s	1565 m/s	1565 m/s
ρ	1930 kg/m^3	1930 kg/m^3	1930 kg/m^3

3.6.3. Model One Simulation Matrix

The "observed data" for Model One (see Figure 3-1) was created by running simulations of the two anisotropic cases, 1-1 and 1-2 (see Table 3-3), to calculate anisotropic GFs. These GFs were simulated using an isotropic explosion source, which can be seen in the left column of Table 3-5. These GFs were then convolved with the STF described in Section 3.3, which resulted in the creation of the "observed" data. The right three columns of Table 3-5 show the GFs of the data sets that were used in the inversions that estimated the MRFs. The GFs were derived from the simulations using the isotropic model and three different sources: an explosion point source, a diagonal moment tensor source, and a general moment tensor source. Inversions were then performed using the "observed" data and the isotropic model GFs to estimate MRFs. A total of six inversions/estimated MRFs were done for Model One, which can be seen in Figure 4-1.

Table 3-5 Simulation matrix for the source used for the calculation of the Model One "observed" data sets. It also shows the GFs that were computed from the Isotropic material parameters. The GFs from the isotropic model are used in the source time function inversion. A total of six inversions/estimated MRFs were done for Model One.

"Observed" Data	Source of Green's functions		
From anisotropic model convolved with STF	Isotropic Model simulated by Explosion Point Source	Isotropic Model simulated by Diagonal Moment Tensor Source	Isotropic Model simulated by General Moment Tensor Source
Case "1-1" - Explosion Source	✓	✓	✓
Case "1-2" - Explosion Source	✓	✓	✓

3.6.4. Model Two Simulation Matrix

The "observed data" for Model Two was created by running simulations of the three anisotropic cases, 2-1, 2-2, and 2-3 (see Section 3.6.2), to calculate anisotropic GFs. These GFs were simulated using an isotropic explosion source, which can be seen in the left column of Table 3-6. There were four different sources used to simulate GFs for each of the Model Two anisotropic material parameter sets. The sources are an explosion source, an earthquake moment source, an explosion plus an earthquake moment source, and a non-isotropic explosion plus earthquake moment source. These GFs were then convolved with the STF described in Section 3.3, which resulted in the creation of the "observed" data. The right three columns of Table 3-6 show the GFs of the data sets that were used in the inversions that estimated the MRFs. The GFs were derived from the simulations using the isotropic model and three different sources: an explosion point source, a diagonal moment tensor source, and a general moment tensor source. Inversions were then performed using the "observed" data and the isotropic model GFs to estimate MRFs. A total

of 12 inversions/estimated MRFs were done for each Model Two anisotropic case. This resulted in a grand total of 36 inversions/estimated MRFs, which can be seen in figures 4-2, 4-3, and 4-4.

Table 3-6 Simulation matrix for the source used for the calculation of the Model Two "observed" data sets. It also shows the GFs that were computed from the Isotropic material parameters. The GFs from the isotropic model are used in the source time function inversion. This table is replicated for each different Model Two anisotropic case, 2-1, 2-2, and 2-3. A total of 12 inversions/estimated MRFs were done for Model Two, case 2-1. A grand total of 36 inversions/estimated MRFs were done for the three cases of Model Two.

"Observed" Data	Source of Green's functions		
From anisotropic model convolved with STF	Isotropic Model simulated by Explosion Point Source	Isotropic Model simulated by Diagonal Moment Tensor Source	Isotropic Model simulated by Full Moment Tensor Source
Expl - Explosion Source	✓	✓	✓
EQ - Earthquake Moment Source	✓	✓	✓
Expl+EQ - Explosion plus Earthquake Moment Source	✓	✓	✓
General - General Moment Source	✓	✓	✓

4. SOURCE TIME FUNCTION INVERSION

To investigate the effects of anisotropy, a source inversion is performed. The source inversion uses an "observed" data set, that is generated externally to the inversion. The "observed" data sets used in the inversions are detailed in Section 3.6. The "observed" data and the synthetic data are time aligned with P-arrival time and inverted using a linear model describing seismic data and the GFs from an isotropic model. The three isotropic model GFs are generated from an explosion point source, a diagonal moment tensor source, and a general moment tensor source. The linear approximation is in the form of:

$$Ax = b \tag{4}$$

Where A is a matrix containing the GFs from the isotropic model, b is a vector containing the "observed" data, and x are the estimated STFs. All receivers are used simultaneously in the inversion. x is found by solving the system of linear equations. See Poppeliers et al., 2019 [9], for more details on the inversion methodology.

4.1. Model One Estimated Moment Rate Functions

The moment rates of estimated sources are compared to the original MRF for the first anisotropic model (1-1) and the second anisotropic model (1-2) of Model One and can be seen in Figure 4-1. The top two plots are for the case where the isotropic model GFs are simulated assuming an explosive source. The middle two plots are for the case where the isotropic model GFs are simulated using a diagonal moment tensor source with, (M_{XX}, M_{YY}, and M_{ZZ}). The bottom two plots are for the simulation case where a general moment tensor, (M_{XX}, M_{YY}, M_{ZZ}, M_{XY}, M_{XZ}, and M_{YZ}, respectively), is used as the source (e.g., Aki and Richards, 2002 [1]). As indicated in Section 3.6.1, the difference between the two models is the P-wave speed in the Y- and Z-directions are swapped. As can be seen in Figure 4-1, both the first and second anisotropic models fit the reference MRF reasonably well, but underestimate the amplitude with the fits at 2/3-3/4 of the true amplitude. This bias is probably due to the anisotropy of the "observed" data. Similar biases have been seen even in truly isotropic models when the earth model used to create the "observed" data does not match that of the GFs (Poppeliers and Preston, 2020 [10]). The first anisotropic model overall has better fit with less erroneous MRF energy before or after the reference MRF. The second anisotropic model has more MRF energy before and after the MRF, but this effect decreases as the number of free parameters in the inversion increase (i.e. going from GFs produced from isotropic-only source to full 6-term moment tensor inversion). In all cases, the off-diagonal moment tensor components have small amplitude, and only small variations in the amplitudes of the on-diagonal components are seen. In other words, all cases were able to recover what the actual source was, which for practical purpose was an explosion with the main bias being in the recovered amplitude of the explosion source.

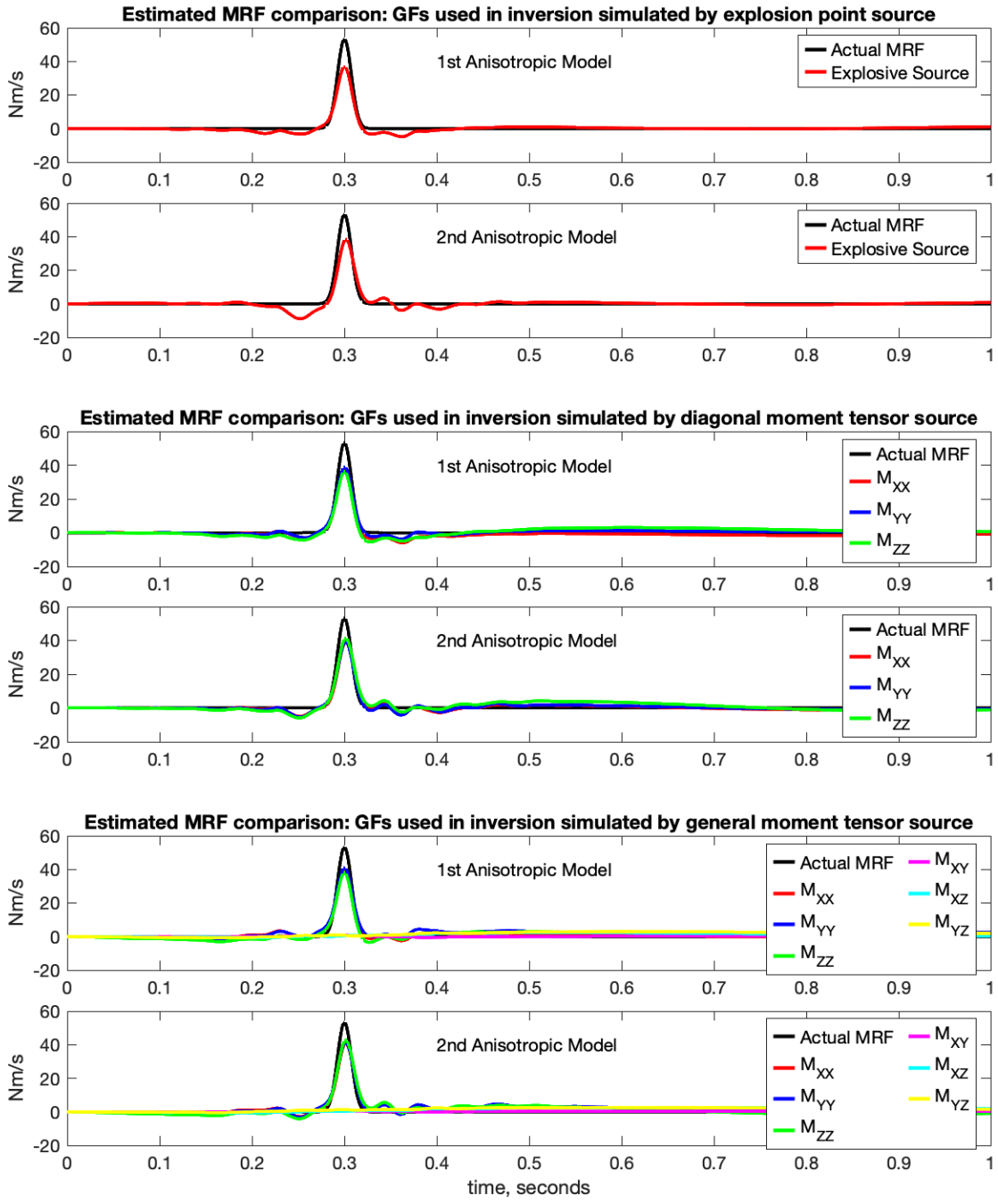

Figure 4-1 Estimated MRFs compared to the MRF for Model 1, cases 1-1 and 1-2. The major take away is that the source inversion reproduces the reference MRF well and that the anisotropy has limited effect.

4.2. Model Two Estimated Moment Rate Functions

Estimated MRFs were computed for Model Two, cases 2-1, 2-2, and 2-3. The moment rates of estimated sources are compared to the original MRF for the three cases of Model Two and can be seen in Figures 4-2, 4-3, and 4-4. The degree of anisotropy increases from case 2-1 to 2-2 to 2-3, the details of which can be seen in Section 3.6.2. In Figures 4-2, 4-3, and 4-4, the figures labeled "Expl" have "observed" data that was created using an explosion source. The figures labeled "EQ" have "observed" data that was created using an earthquake source. The figures labeled "Expl+EQ" have "observed" data that was created using a source comprising both an explosion and an earthquake. The figures labeled "General" have "observed" data that was created using a general moment tensor source. The MRF estimated by inverting the "observed" data in the figures in the left column were estimated using GFs that were simulated by an explosion point source in an isotropic media. The inversion in the figures in the middle column were estimated using GFs that were simulated by a partial moment tensor source (M_{XX}, M_{YY}, and M_{ZZ}) in an isotropic media. The inversions use GFs simulated by a full moment tensor source (M_{XX}, M_{YY}, M_{ZZ}, M_{XY}, M_{XZ}, and M_{YZ}, respectively) in an isotropic media.

4.2.1. Case 2-1

The moment rates of estimated sources are compared to the original MRF for the Model Two, case 2-1 and are seen in Figure 4-2. The results in the figure labeled "Expl" are directly comparable to the results in Figure 4-1 labeled "1st Anisotropic Model", since the wave speed parameters in this case are the same as the parameters in Model One, case 1-1. Observations of the different sources used to simulate the "observed" data GFs are as follows:

- "Expl": Same general observations as for Model 1. All three GF sets in general properly recover the reference MRF. Main differences again are underestimate at the peak and early and late time energy on the recovered MRF not present in the reference. Very little energy is observed on the estimated MRFs corresponding to the off diagonals of the general moment tensor or variation in on-diagonal components, so it looks for all practical purposes like an explosion.

- "EQ": We would not expect good fits for explosion-only or on-diagonal GFs, and indeed we do not get good fits for those. The inversion using the full moment tensor source model does a nice job of fitting the MRFs corresponding to the M_{XY} component with the MRFs corresponding to the other tensor components being smaller, but there are still sizeable erroneous MRF amplitudes corresponding to the on diagonal components of the moment tensor.

- "Expl+EQ": Basically a combination of "Expl" and "EQ" cases above: Reasonably good fit to the on-diagonal components for all three GF sets and a good fit to the M_{XY} in the full moment tensor case, with very little bleed off into other off-diagonal components. There is a fairly strong erroneous late-time negative amplitude on the on-diagonal components just after the main pulse.

- "General": This source model is more affected by low-frequency noise in the recovered MRFs compared to the others. The fact that there is a lot of on-diagonal energy in the actual MRF is well-recovered; however, the relative amplitudes of the on-diagonal components of the moment tensor are not recovered as well. The off-diagonal components are generally well-recovered, with the MRF corresponding to the M_{XY} component of the tensor being properly identified as the true off-diagonal component with other off-diagonal components having relatively small MRF amplitudes.

4.2.2. Case 2-2

The moment rates of the estimated sources for Model Two, case 2-2, compared to the reference MRF can be seen in Figure 4-3. The observations for this case are very similar to case 2-1 (see Section 4.2.1). There are two primary differences in this case compared to Case 2-1. First, the M_{XY} component is not as well-recovered as in Case 2-1 with a smaller recovered amplitude and broader MRF than the reference. Second, the low frequency noise in the “General” source case is stronger, but it appears the relative amplitudes of the on-diagonal components may be better recovered in this case than the last.

4.2.3. Case 2-3

The moment rates of the estimated sources for Model Two, case 2-3, compared to the actual MRF can be seen in Figure 4-4. The "Expl" source model is about the same as in the previous two cases (see Sections 4.2.1 and 4.2.2). However, the "EQ" source is very poorly recovered, with the M_{XY} component and on-diagonal components erroneously showing nearly the same amplitudes. For the "Expl+EQ" case, the on-diagonal components generally recover smaller amplitude than in previous cases with some extra erroneous complexity especially with the explosion-only GFs inversion. The M_{XY} component in this source model is also poorly recovered. Finally, for the "General" source model, there is more low-frequency noise manifested than in the other models. The amplitudes of the on-diagonal components are not as well recovered in both an absolute and relative sense, with the addition of erroneous complexity especially later in time. The explosion-only GF recovery is especially poor with two major pulses recovered, the latter of which actually has higher amplitude than the one that aligns with the reference pulse. Again, the M_{XY} component is poorly recovered, but there is still little amplitude on the other off-diagonal components.

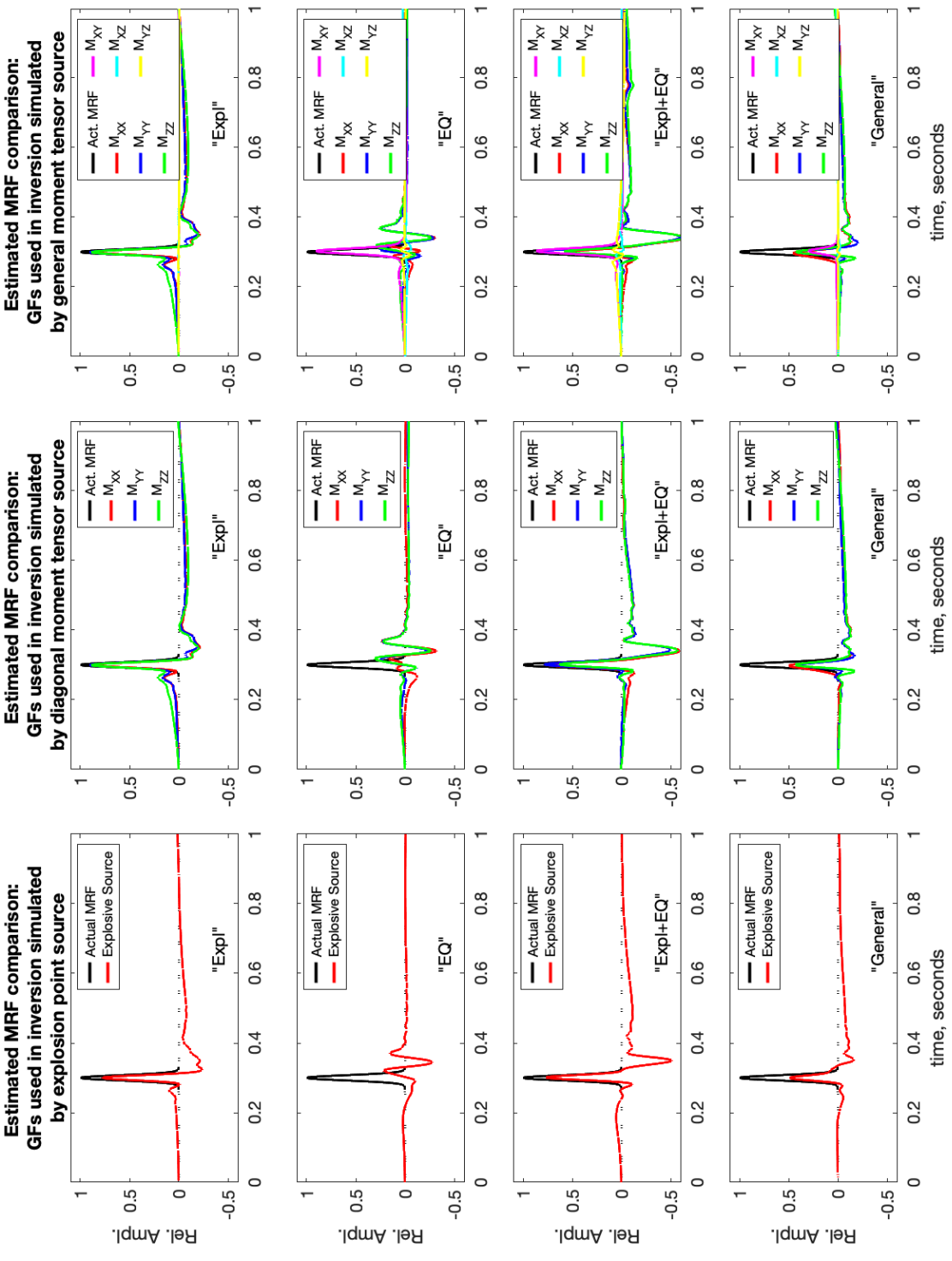

Figure 4-2 Estimated MRFs compared to the original MRF for Model Two, case 2-1.

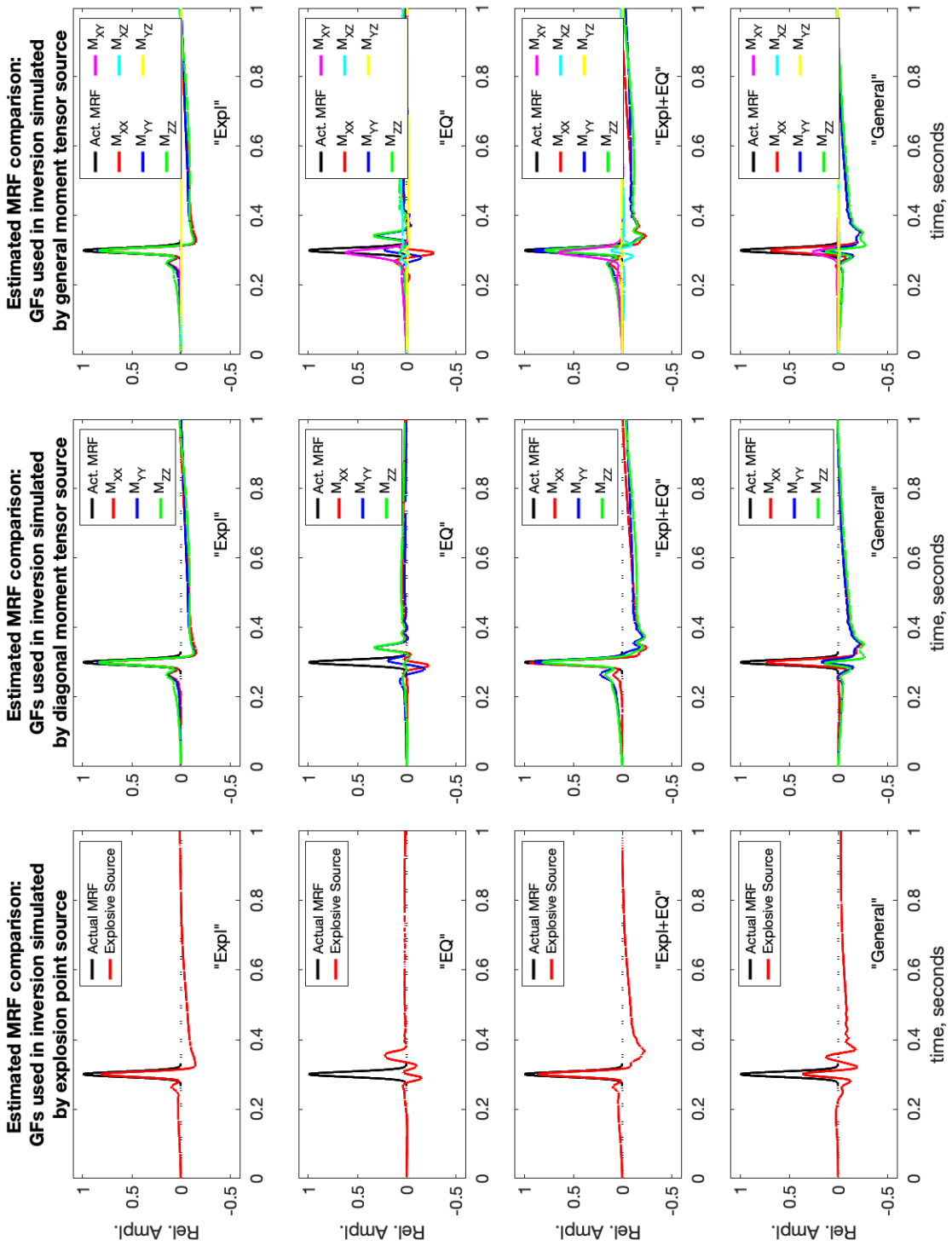

Figure 4-3 Estimated MRFs compared to the original MRF for Model Two, case 2-2.

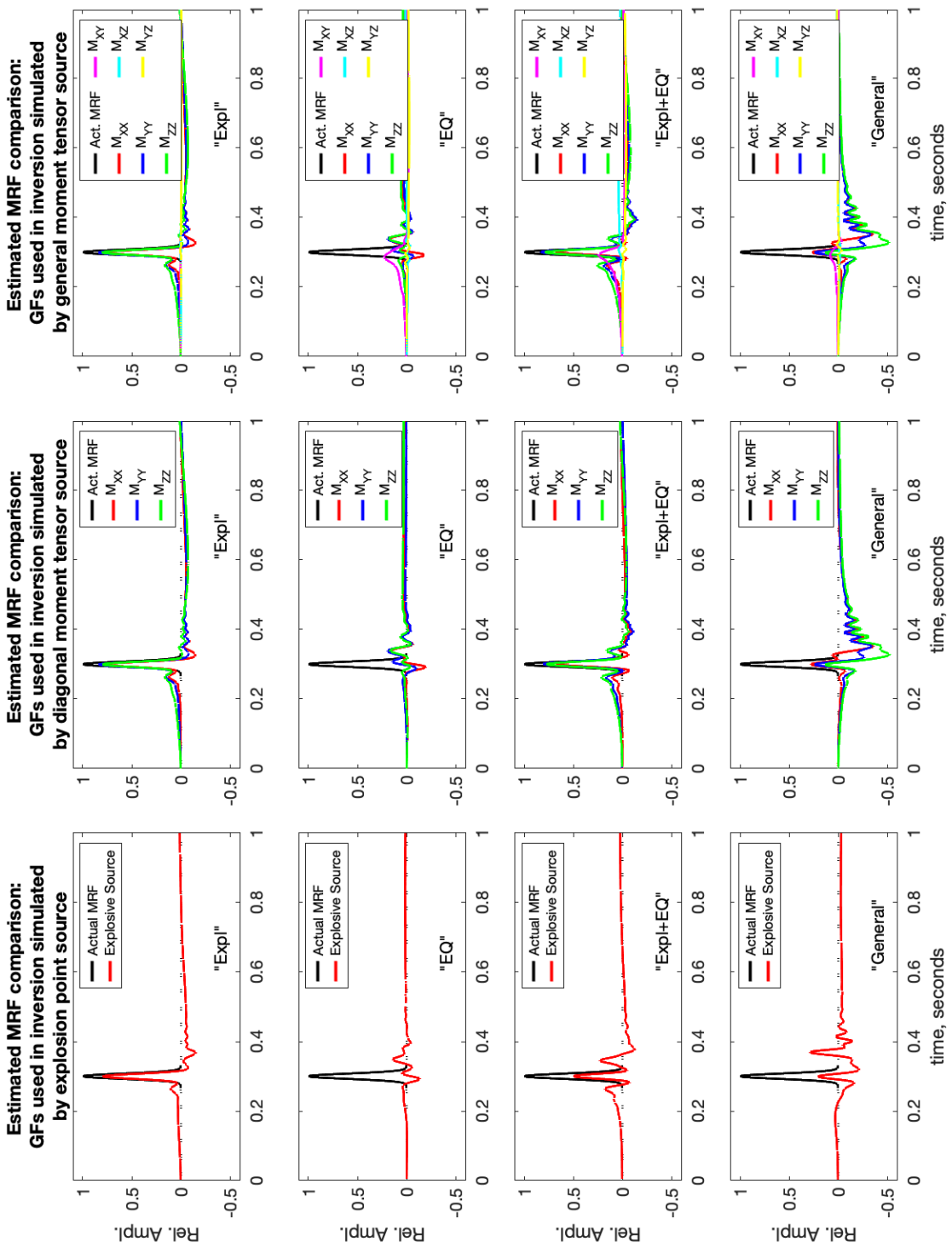

Figure 4-4 Estimated MRFs compared to the original MRF for Model Two, case 2-3.

5. DISCUSSION

To check how well the inversion worked, the estimated MRFs were then convolved with the isotropic GFs used in the inversion. The resulting predicted seismograms were then individually normalized and plotted as record sections with the "observed" data. There are a large number of these plots, so only a few will be shown in this section. The suite of plots is included in the Appendix.

Figures 5-1 and 5-2 are the V_X and V_Z record sections of the isotropic GFs convolved with the estimated STF for Model Two, Case 2-3. The plots show the seismograms for all three source types used in generating the isotropic GFs (explosion, partial moment, and full moment source) with the seismograms for the 'observed' data. The plots labeled "Expl", "EQ", "Expl+EQ", and "General" correspond to the four different source types used to create the "observed" data (see Section 3.6.3). The seismograms in Figure 5-1 are from the receiver Line 5 and the seismograms in Figure 5-2 are from receiver Line 6. Line 5 has an azimuth of 270° and Line 6 has an azimuth of 205° (see Figure 3-2).

Because the observed and predicted data were time aligned to the first arriving P-energy, the P-wave arrivals tend to be better fit and later arrivals have a significantly degraded fit. Anisotropy introduces systematic time variations in the arrival of P, S waves, and surface waves. S-waves are additionally split into two phases that can arrive at different times with different amplitudes depending on the receiver component and direction. Thus, S-waves and surface waves produced by an anisotropic model are much harder if not impossible to fit well with a purely isotropic model especially across multiple components and receivers. Because of all this and the fact that explosions are dominated by compressive energy, by time aligning on the P-wave we are maximizing the ability of the inversion to correctly obtain isotropic sources at the expense of other source types.

Erroneous early and late time signals on the recovered STFs are due to the purely isotropic model attempting to fit P and S arrivals that have varying arrival times with source-receiver direction. Inversion models using all six GF components (i.e. having the most degrees of freedom) are most able to try to fit these arrivals that the physics of the isotropic GFs cannot replicate, causing increased variability and erroneous recovered pulses.

As the complexity of the source model increases along with the anisotropy of the Earth, the less well the inversion is able to produce results that fit the observations. For truly "simple" sources such as pure explosions, the inversions were able to estimate the MRFs remarkably well even in the earth models with the highest anisotropy evaluated. This result was most likely aided by the fact that we time-aligned the observed and synthetic P-waves before inversion. However, even a "simple" source like the earthquake which was pure M_{XY} (strike-slip) was well-recovered in the earth model with the lowest amount of anisotropy, and in that case was able to properly disambiguate earthquake plus explosion sources. With greater anisotropy, though, the quality (or accuracy) of the results was reduced. The fact that we did not see a significant amount of energy bleed onto other off-diagonal components may be partially due to the source-receiver geometry which would maximize sensitivity to the M_{XY} component relative to the M_{XZ} or M_{YZ} components; however, there should still be sufficient sensitivity to indicate that there cannot be a

large trade-off among the off-diagonal components. Among the on-diagonal components, relative amplitudes among the components were not as well recovered compared to the fact that there was a large amount of isotropic energy in the source.

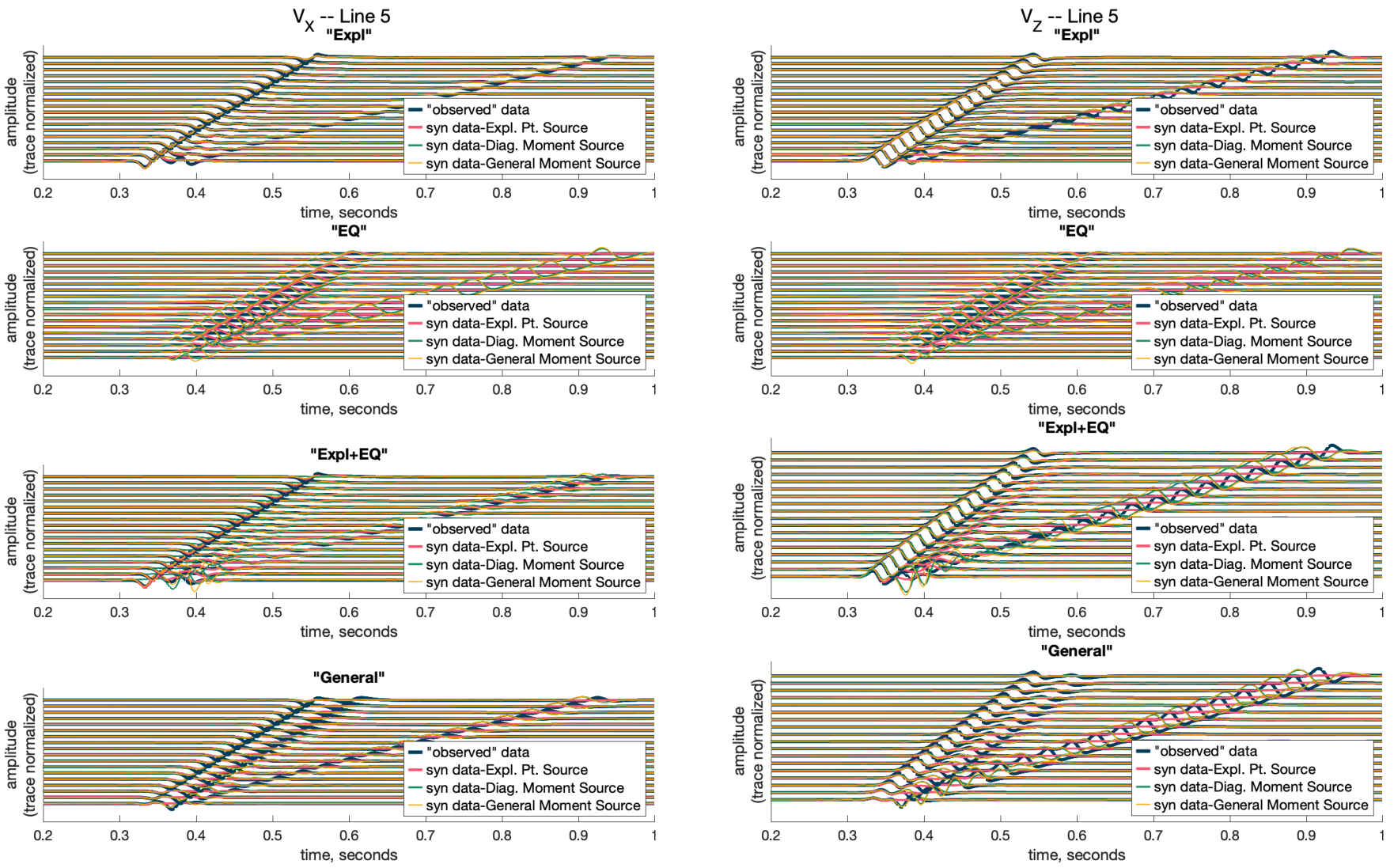

Figure 5-1 V_X and V_Z record sections of the isotropic GFs convolved with the estimated STF for Model Two, Case 2-1. The plots show the seismograms for all three source types used in generating the isotropic GFs (explosion, partial moment, and full moment source) with the seismograms for the 'observed' data. The plots labeled "Expl", "EQ", "Expl+EQ", and "General" correspond to the four different source types used to create the "observed" data (see Section 3.6.4). These seismograms are for receiver Line 5.

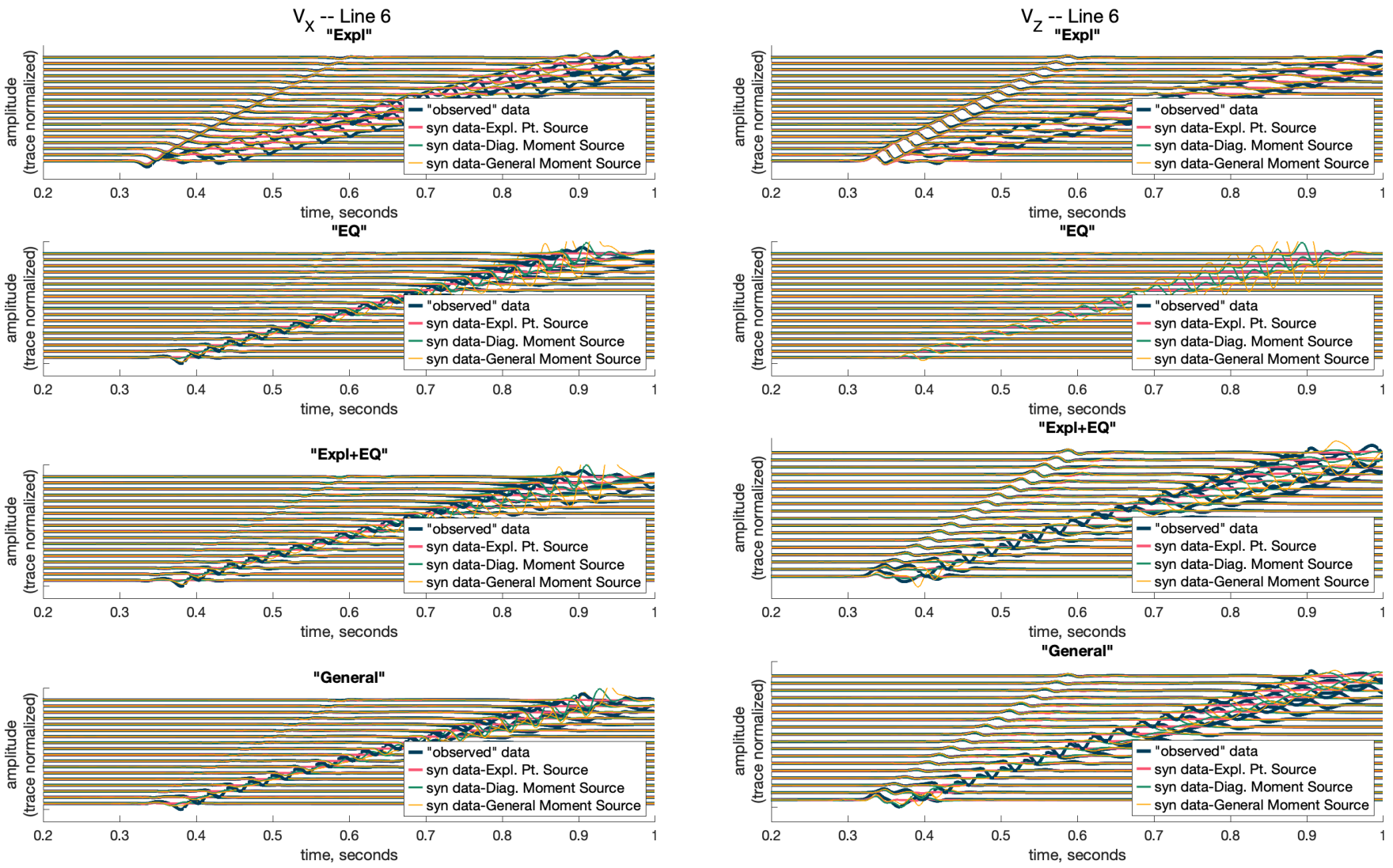

Figure 5-2 V_X and V_Z record sections of the isotropic GFs convolved with the estimated STF for Model Two, Case 2-1. The plots show the seismograms for all three source types used in generating the isotropic GFs (explosion, partial moment, and full moment source) with the seismograms for the 'observed' data. The plots labeled "Expl", "EQ", "Expl+EQ", and "General" correspond to the four different source types used to create the "observed" data (see Section 3.6.4). These seismograms are for receiver Line 6.

6. SUMMARY

We investigated the errors and biases that result from modeling a non-isotropic medium as an isotropic medium. This was done by computing “observed data” by using synthetic, anisotropic simulations with the assumption of an orthorhombic, anisotropic earth model. The initial thought was that when an earth model is assumed to be isotropic, the characterization of the seismic sources would be affected by the shear waves produced in an anisotropic model even when the source is an isotropic explosion. The results of the study did not bear this out for the model/source configurations that we investigated. The estimated STFs did a fairly good job of matching the actual STF and clearly defined the type of source. The amplitudes, while generally reasonable, were inaccurate. This bias was most likely introduced due to the anisotropic nature of the "observed" data not matching the isotropic Earth structure used in making the GFs.

The main take-away is that time-aligning to the P-wave before inversion appears to allow good recovery of true explosive source types even in anisotropic models (i.e. good true positive rate). However, there is potential for false positives, where it appears there is isotropic seismic energy, but in actuality there is not (e.g. isotropic energy recovered for pure earthquake source). For relatively low amounts of anisotropy and assuming the full moment tensor can be recovered, relationships in time among the different components could help distinguish false from true positives. However, these time relationships break down with greater amounts of anisotropy. We did not model any cases that showed no isotropic energy when in actuality there was some (no false negatives), and we observed little interference into off-diagonal moment tensor components. The primary issue we observed was that the amplitude of the recovered on-diagonal components could be biased. However, this can be an issue whenever the earth model used to make the GFs does not match the true earth, even in truly isotropic earth models (e.g. Poppeliers and Preston, 2020 [10]).

REFERENCES

[1] K. Aki and P.G. Richards. *Quantitative Seismology, Second Edition*. University Science Books, Sausalito, CA, 2002.

[2] J-P. Berenger. A perfectly matched layer for the absorption of electromagnetic waves. *J. Comp. Phys.*, 114:185–200, 1994.

[3] S.P. Cheadle, R.J. Brown, and D.C. Lawton. Orthorhombic anisotropy: A physical modeling study. *Geophysics*, 56:1603–1613, 1991.

[4] H.H. Hess. Seismic anisotropy of the uppermost mantle under oceans. *Nature*, 203:629–631, 1964.

[5] J.E. Johnston and N.I. Christensen. Seismic anisotropy of shales. *J. Geophys. Res., Solid Earth*, 100(B4):5991–6003, 1995.

[6] D. Komatitsch and R. Martin. an unsplit convolutional perfectly matched layer improved at grazing incidence for the seismic wave equation. *Geophysics*, 72(5):SM155–SM167, 2007.

[7] K.C. Meza-Fajardo and A.S. Papgeorgiou. A non-convolutional, split-field, perfectly matched layer for wave propagation in isotropic and anisotropic elastic media: Stability analysis. *Bull. Seis. Soc. Am.*, 98(4):1811–1836, 2008.

[8] M.J.P. Musgrave. *Crystal Acoustics*. Holden Day, San Francisco, CA, 1970.

[9] C. Poppeliers, K.A. Aur, and L.A. Preston. The relative importance of assumed infrasound source terms and effests of atmospheric models on the linear inversion of infrasound time series at the source physics experiment. *Bull. Seis. Soc. Am.*, 109(1):463–475, 2019.

[10] C. Poppeliers and L.A. Preston. The effects of model uncertainty on the inversion of seismic data for seismic source functions. *Geophys. J. Int.*, 224(1):100–120, 2020.

[11] L.A. Preston. Pararhombi: Parallel implementation of 3-d seismic wave propagation in orthorhombic media. Technical Report SAND2018-9477, Sandia National Laboratories, Albuquerque, NM, August 2018.

[12] M. Schoenberg and K. Helbig. Orthorhombic media: Modeling elastic wave behavior in a vertically fractured earth. *Geophysics*, 62(6):1954–1974, 1997.

[13] I. Tsvankin. Anisotropic parameters and p-wave velocity for orthorhombic media. *Geophysics*, 62(4):1292–1309, 1997.

[14] J. Virieux. P-sv wave propagation in heterogeneous media: Velocity-stress finite-difference method. *Geophysics*, 51:889–901, 1986.

APPENDIX A. TRACE PLOTS

The plots in the appendix are the V_X and V_Z record sections of the isotropic GFs convolved with the estimated STF for all of the cases in both Model One and Model Two. The plots show the seismograms for all the source types used in generating the isotropic GFs (explosion, partial moment, and full moment source) with the seismograms for the 'observed' data. The figure captions have the explanation of the plots.

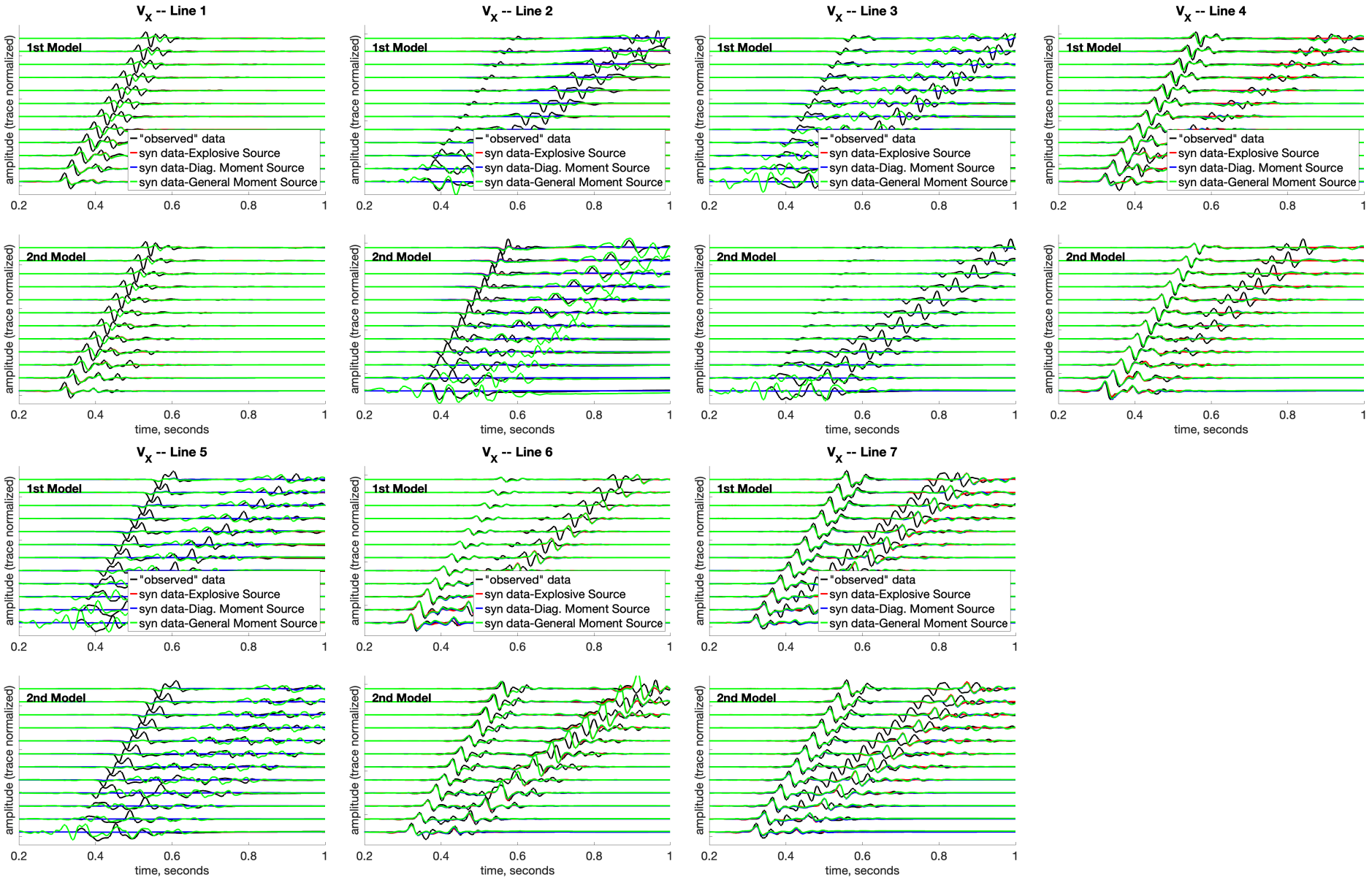

Figure A-1 V_X record sections of the isotropic GFs convolved with the estimated STF for Model One. The plots show the seismograms for all three source types used in generating the isotropic GFs (explosion, partial moment, and full moment source) with the seismograms for the 'observed' data. The plots labeled "1st Model" are case 1-1 and those labeled "2nd Model' are case 1-2. There are a total of seven receiver lines. The plots are organized by receiver line.

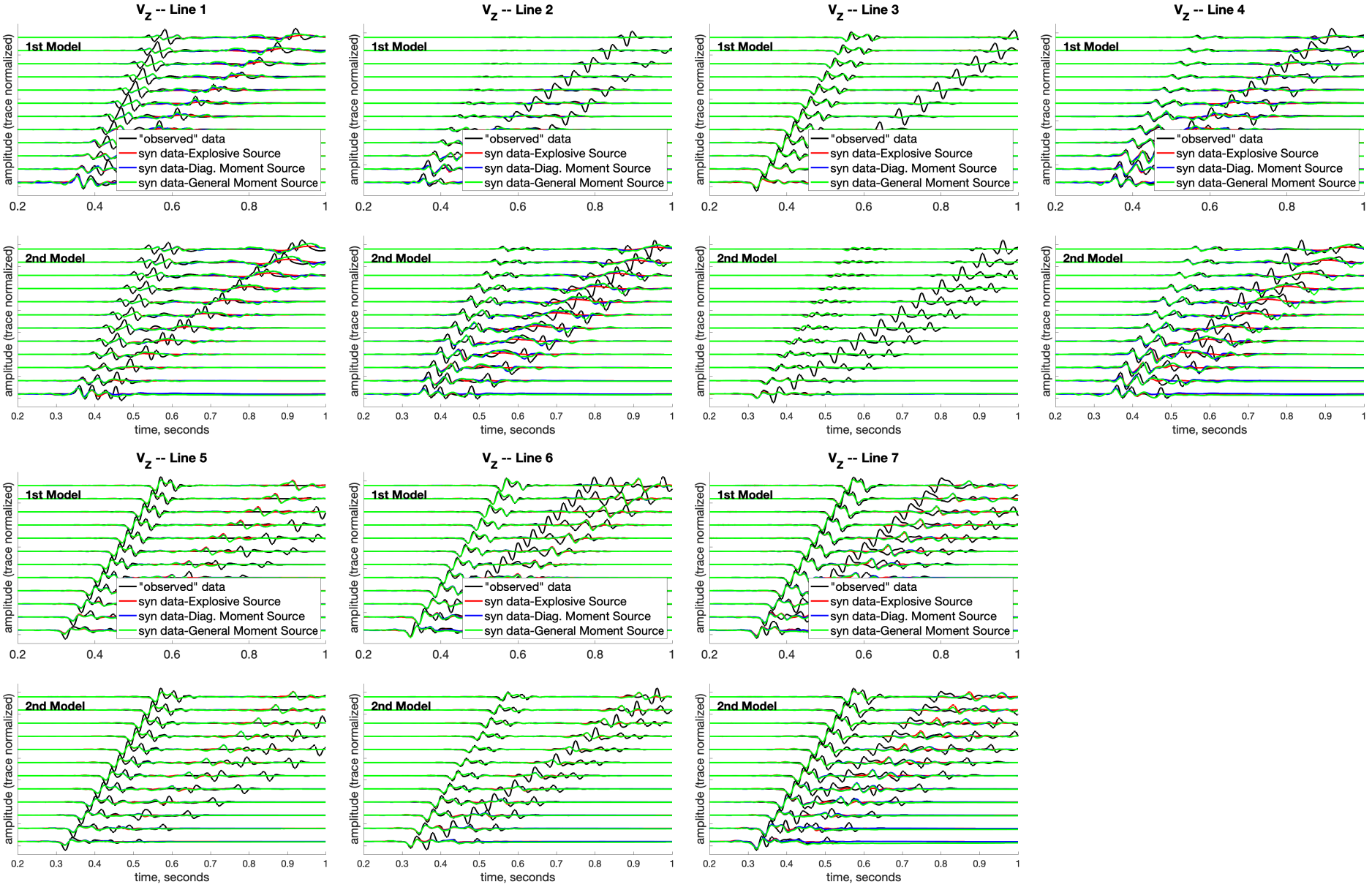

Figure A-2 V_Z **record sections of the isotropic GFs convolved with the estimated STF for Model One. The plots show the seismograms for all three source types used in generating the isotropic GFs (explosion, partial moment, and full moment source) with the seismograms for the 'observed' data. The plots labeled "1st Model" are case 1-1 and those labeled "2nd Model' are case 1-2. There are a total of seven receiver lines. The plots are organized by receiver line.**

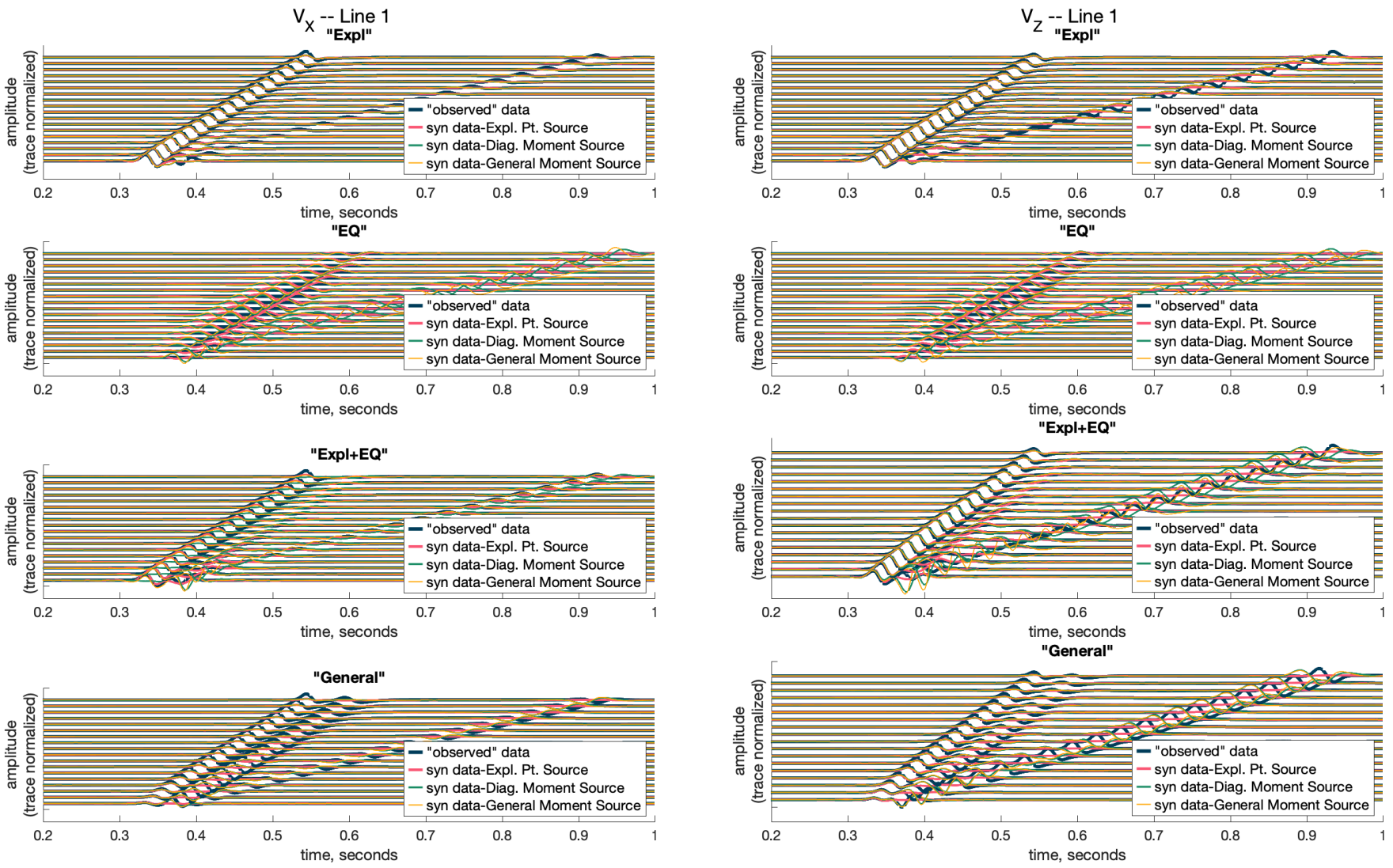

Figure A-3 V_X and V_Z record sections of the isotropic GFs convolved with the estimated STF for Model Two, Case 2-1. The plots show the seismograms for all three source types used in generating the isotropic GFs (explosion, partial moment, and full moment source) with the seismograms for the 'observed' data. The plots labeled "Expl", "EQ", "Expl+EQ", and "General" correspond to the four different source types used to create the "observed" data (see Section 3.6.4). These seismograms are for receiver Line 1.

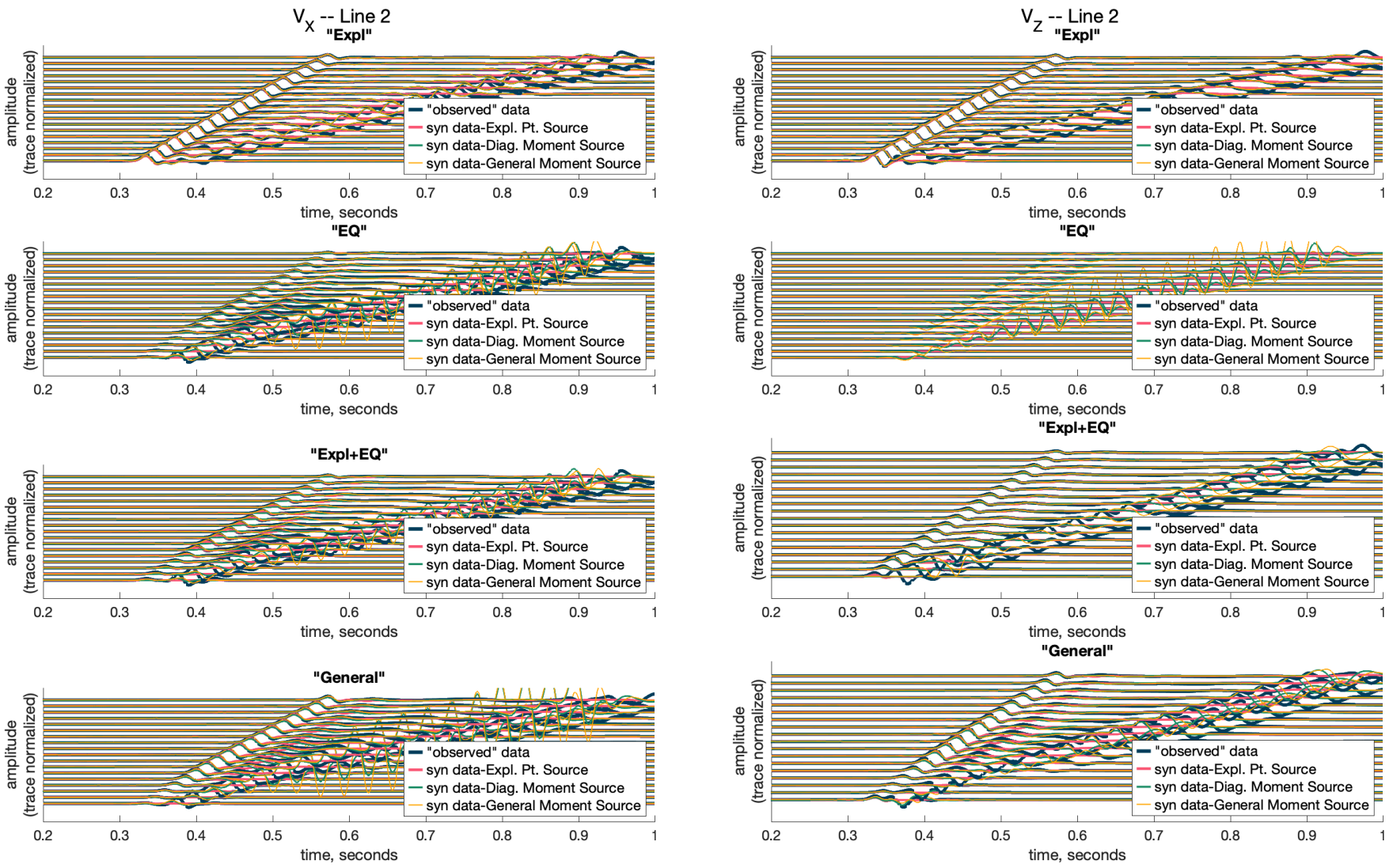

Figure A-4 V_X **and** V_Z **record sections of the isotropic GFs convolved with the estimated STF for Model Two, Case 2-1. The plots show the seismograms for all three source types used in generating the isotropic GFs (explosion, partial moment, and full moment source) with the seismograms for the 'observed' data. The plots labeled "Expl", "EQ", "Expl+EQ", and "General" correspond to the four different source types used to create the "observed" data (see Section 3.6.4). These seismograms are for receiver Line 2.**

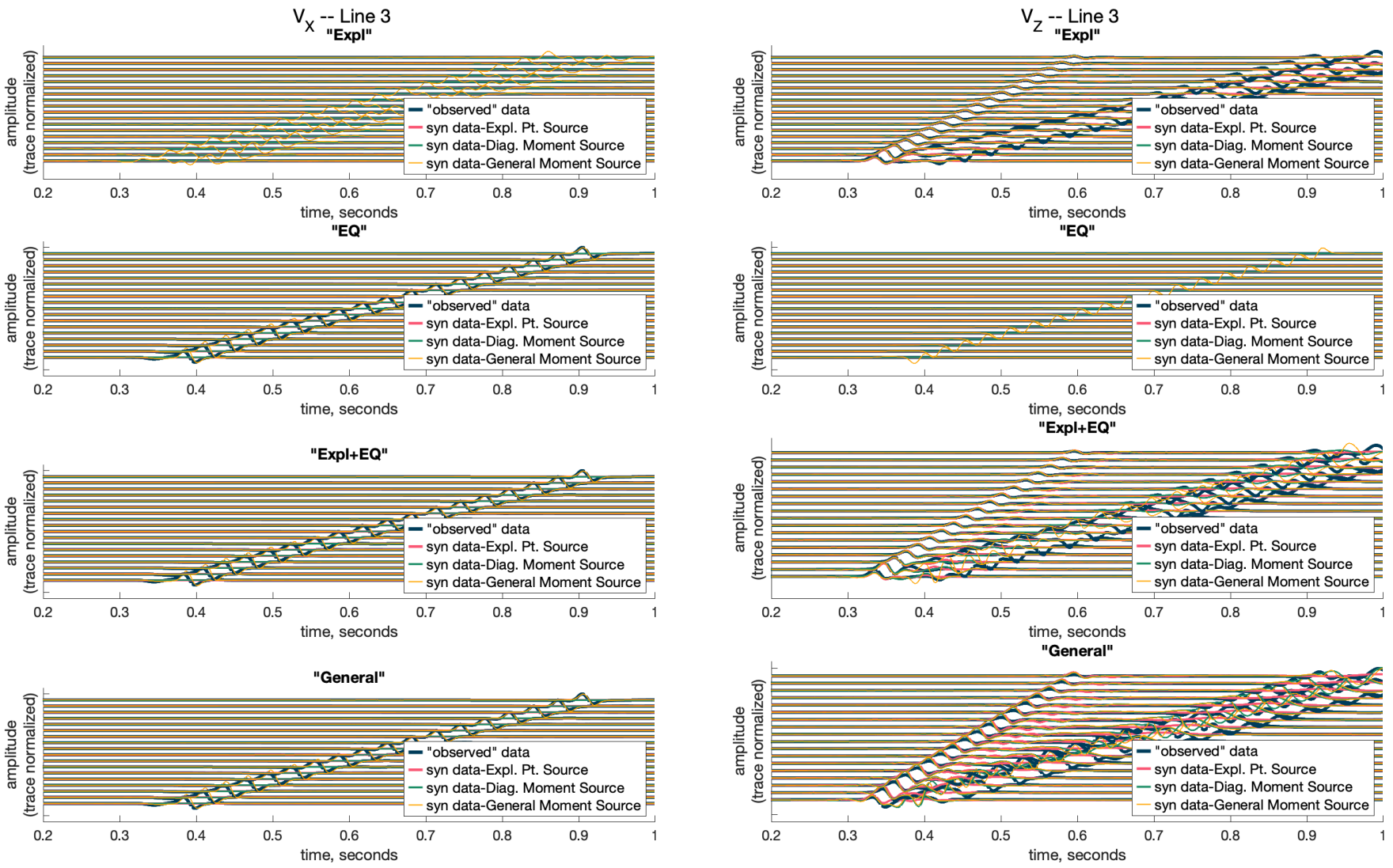

Figure A-5 V_X and V_Z record sections of the isotropic GFs convolved with the estimated STF for Model Two, Case 2-1. The plots show the seismograms for all three source types used in generating the isotropic GFs (explosion, partial moment, and full moment source) with the seismograms for the 'observed' data. The plots labeled "Expl", "EQ", "Expl+EQ", and "General" correspond to the four different source types used to create the "observed" data (see Section 3.6.4). These seismograms are for receiver Line 3.

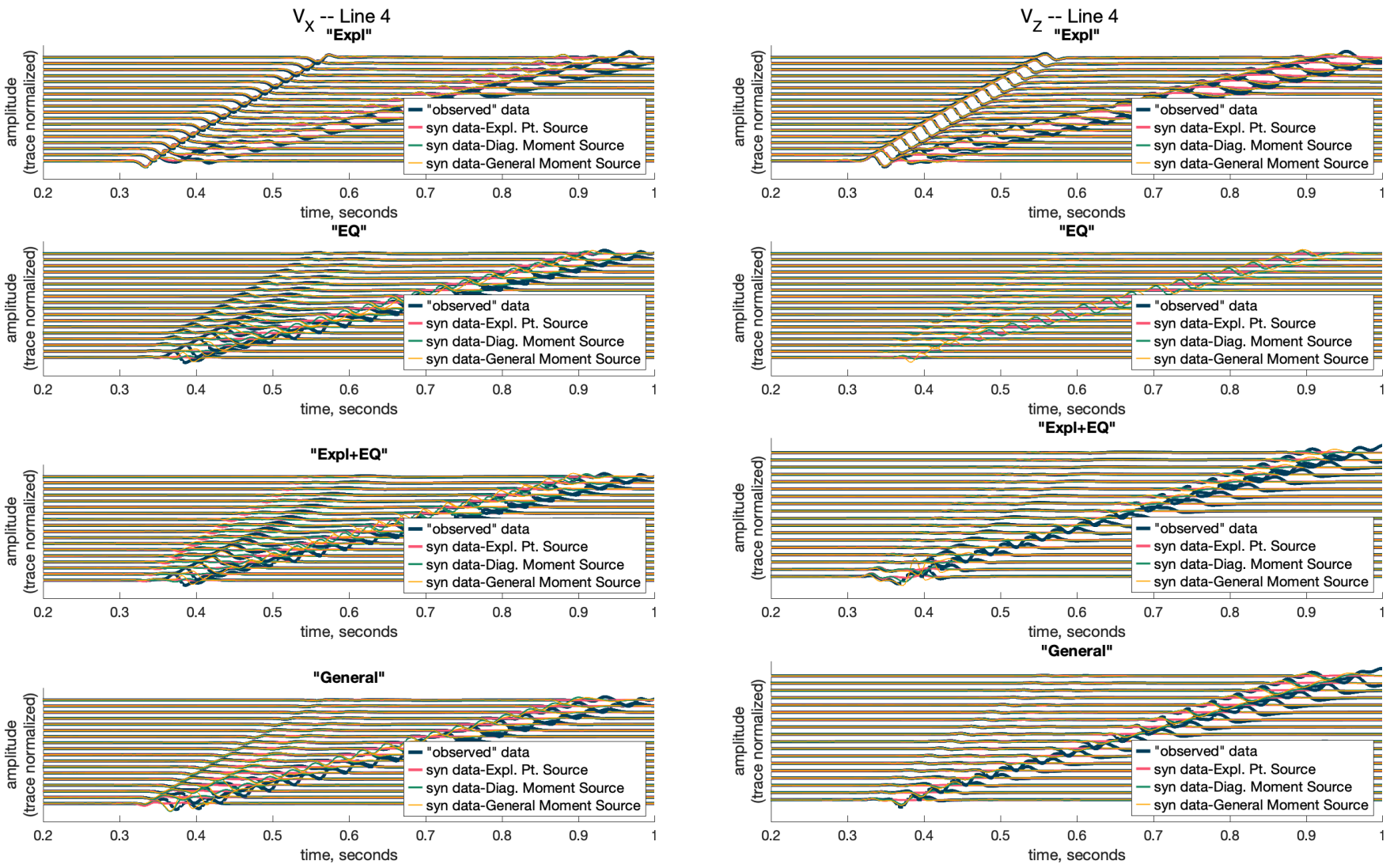

Figure A-6 V_X and V_Z record sections of the isotropic GFs convolved with the estimated STF for Model Two, Case 2-1. The plots show the seismograms for all three source types used in generating the isotropic GFs (explosion, partial moment, and full moment source) with the seismograms for the 'observed' data. The plots labeled "Expl", "EQ", "Expl+EQ", and "General" correspond to the four different source types used to create the "observed" data (see Section 3.6.4). These seismograms are for receiver Line 4.

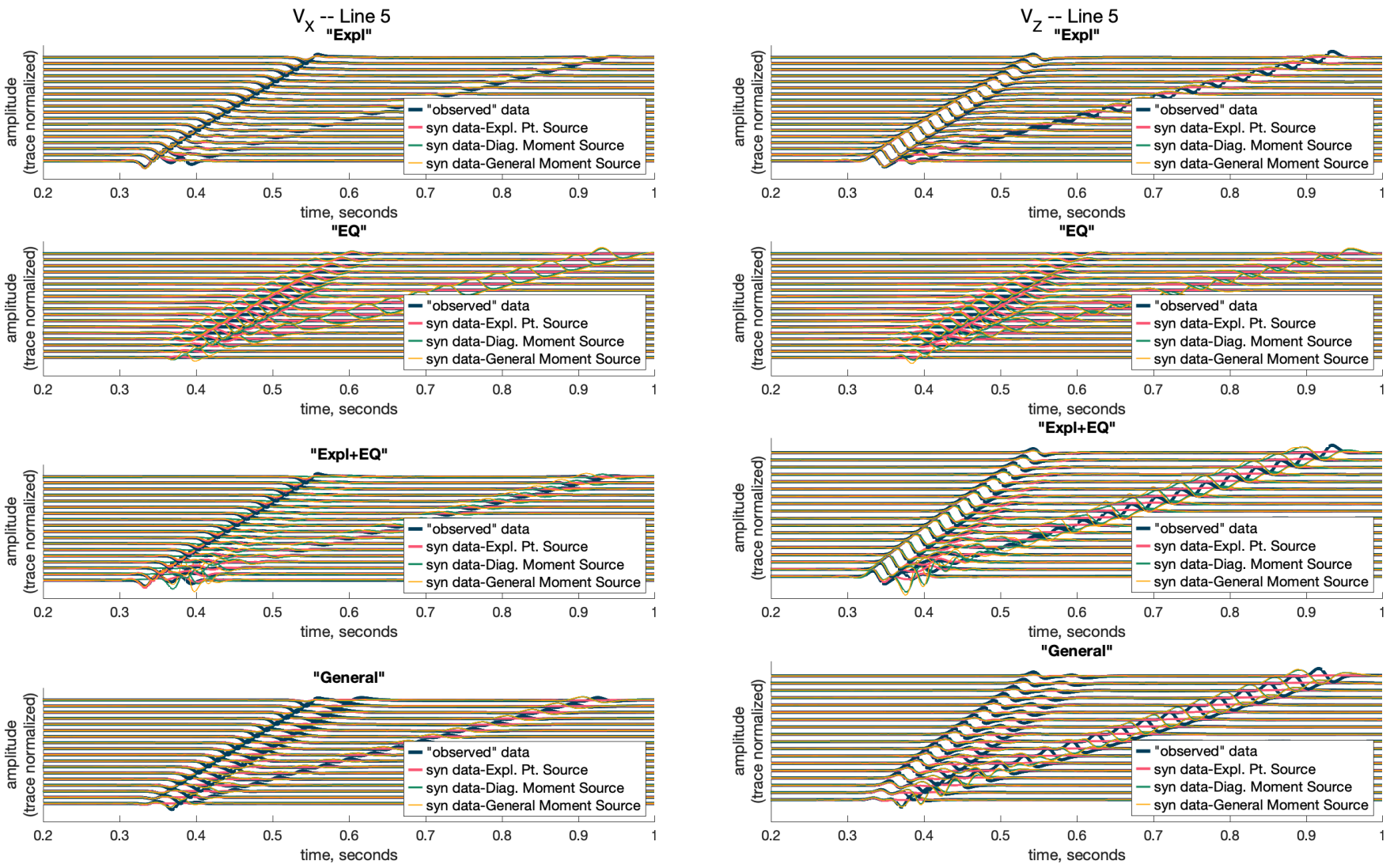

Figure A-7 V_X **and** V_Z **record sections of the isotropic GFs convolved with the estimated STF for Model Two, Case 2-1. The plots show the seismograms for all three source types used in generating the isotropic GFs (explosion, partial moment, and full moment source) with the seismograms for the 'observed' data. The plots labeled "Expl", "EQ", "Expl+EQ", and "General" correspond to the four different source types used to create the "observed" data (see Section 3.6.4). These seismograms are for receiver Line 5.**

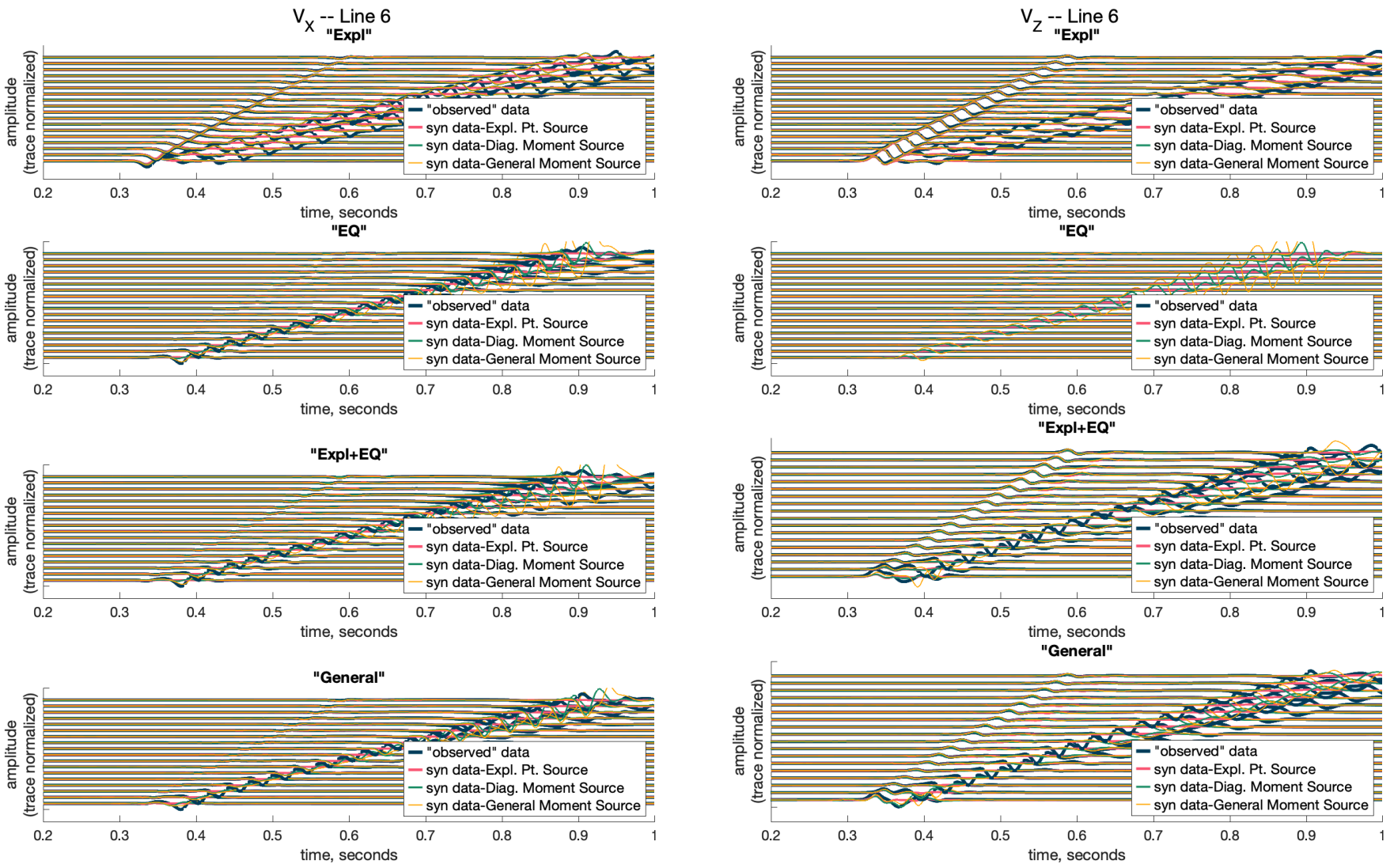

Figure A-8 V_X and V_Z record sections of the isotropic GFs convolved with the estimated STF for Model Two, Case 2-1. The plots show the seismograms for all three source types used in generating the isotropic GFs (explosion, partial moment, and full moment source) with the seismograms for the 'observed' data. The plots labeled "Expl", "EQ", "Expl+EQ", and "General" correspond to the four different source types used to create the "observed" data (see Section 3.6.4). These seismograms are for receiver Line 6.

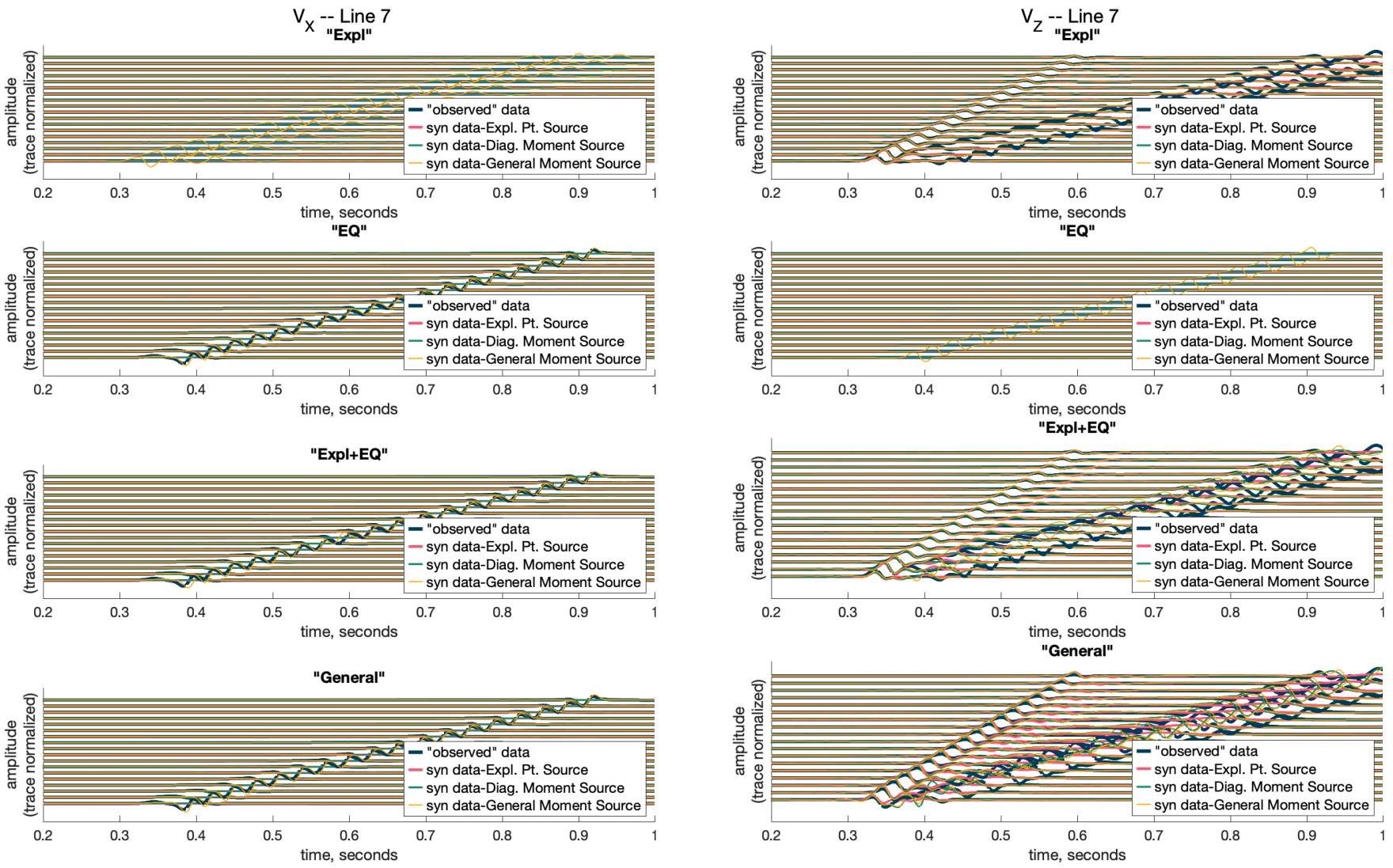

Figure A-9 V_X and V_Z record sections of the isotropic GFs convolved with the estimated STF for Model Two, Case 2-1. The plots show the seismograms for all three source types used in generating the isotropic GFs (explosion, partial moment, and full moment source) with the seismograms for the 'observed' data. The plots labeled "Expl", "EQ", "Expl+EQ", and "General" correspond to the four different source types used to create the "observed" data (see Section 3.6.4). These seismograms are for receiver Line 7.

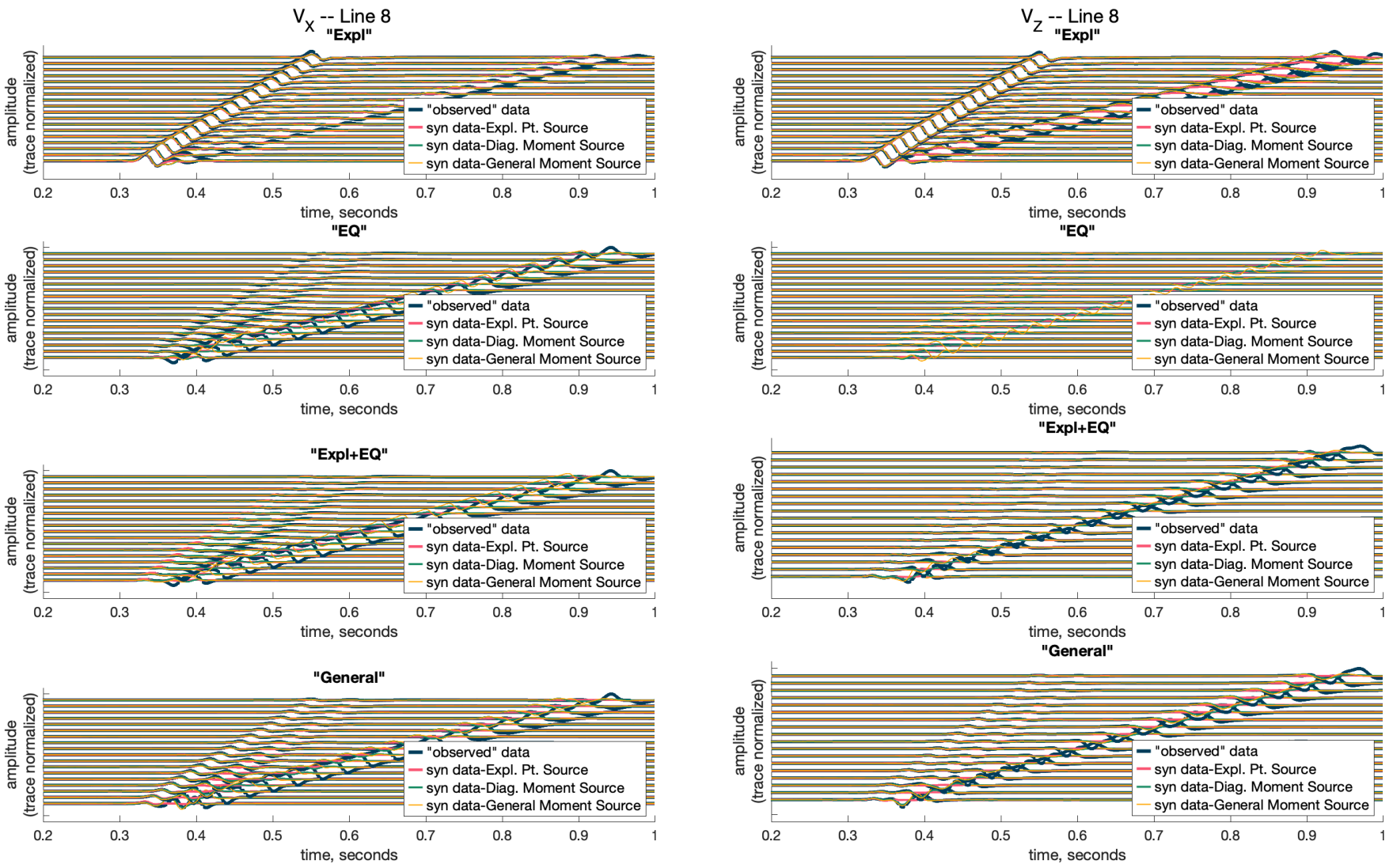

Figure A-10 V_X **and** V_Z **record sections of the isotropic GFs convolved with the estimated STF for Model Two, Case 2-1. The plots show the seismograms for all three source types used in generating the isotropic GFs (explosion, partial moment, and full moment source) with the seismograms for the 'observed' data. The plots labeled "Expl", "EQ", "Expl+EQ", and "General" correspond to the four different source types used to create the "observed" data (see Section 3.6.4). These seismograms are for receiver Line 8.**

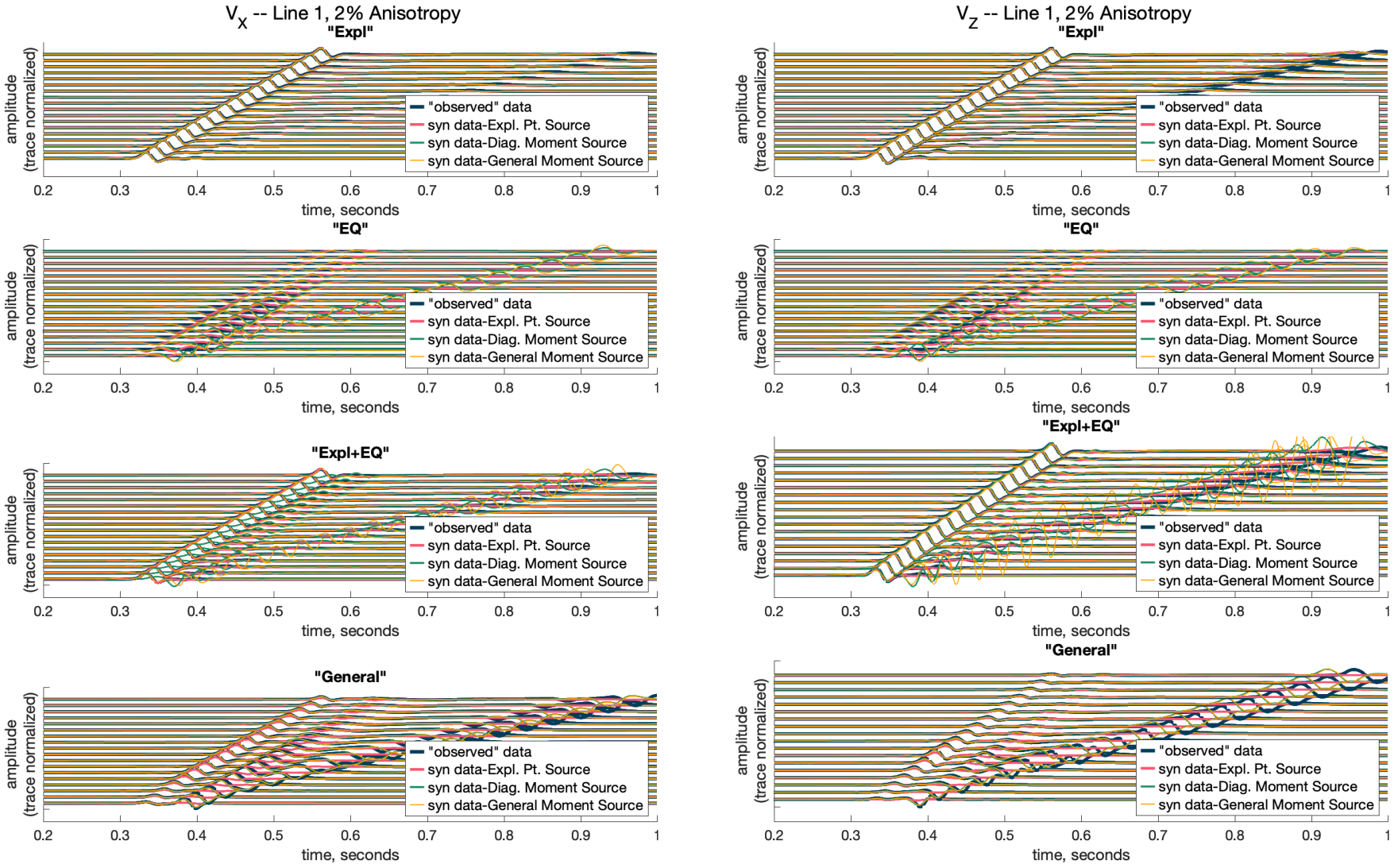

Figure A-11 V_X **and** V_Z **record sections of the isotropic GFs convolved with the estimated STF for Model Two, Case 2-2. The plots show the seismograms for all three source types used in generating the isotropic GFs (explosion, partial moment, and full moment source) with the seismograms for the 'observed' data. The plots labeled "Expl", "EQ", "Expl+EQ", and "General" correspond to the four different source types used to create the "observed" data (see Section 3.6.4). These seismograms are for receiver Line 1.**

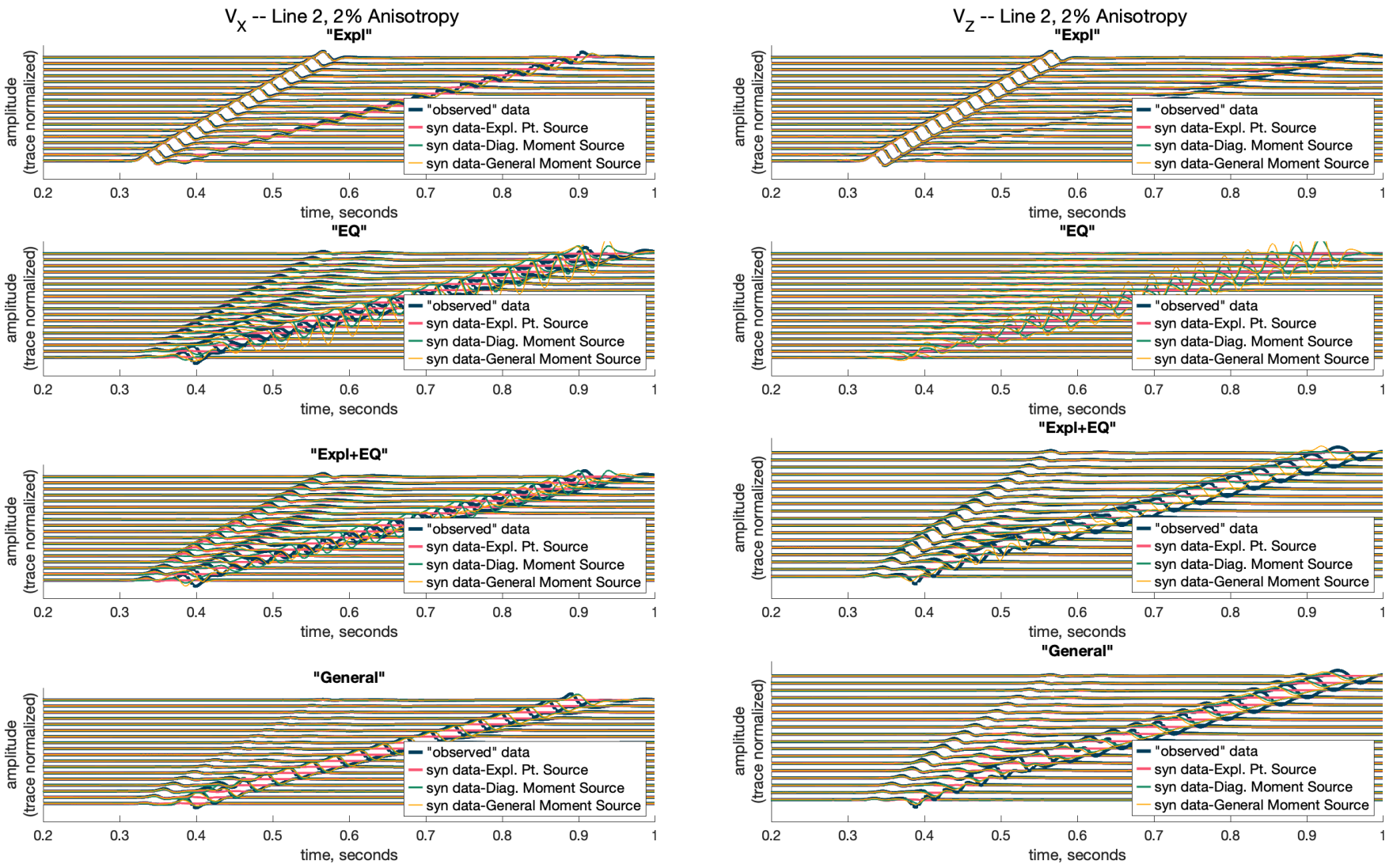

Figure A-12 V_X **and** V_Z **record sections of the isotropic GFs convolved with the estimated STF for Model Two, Case 2-2. The plots show the seismograms for all three source types used in generating the isotropic GFs (explosion, partial moment, and full moment source) with the seismograms for the 'observed' data. The plots labeled "Expl", "EQ", "Expl+EQ", and "General" correspond to the four different source types used to create the "observed" data (see Section 3.6.4). These seismograms are for receiver Line 2.**

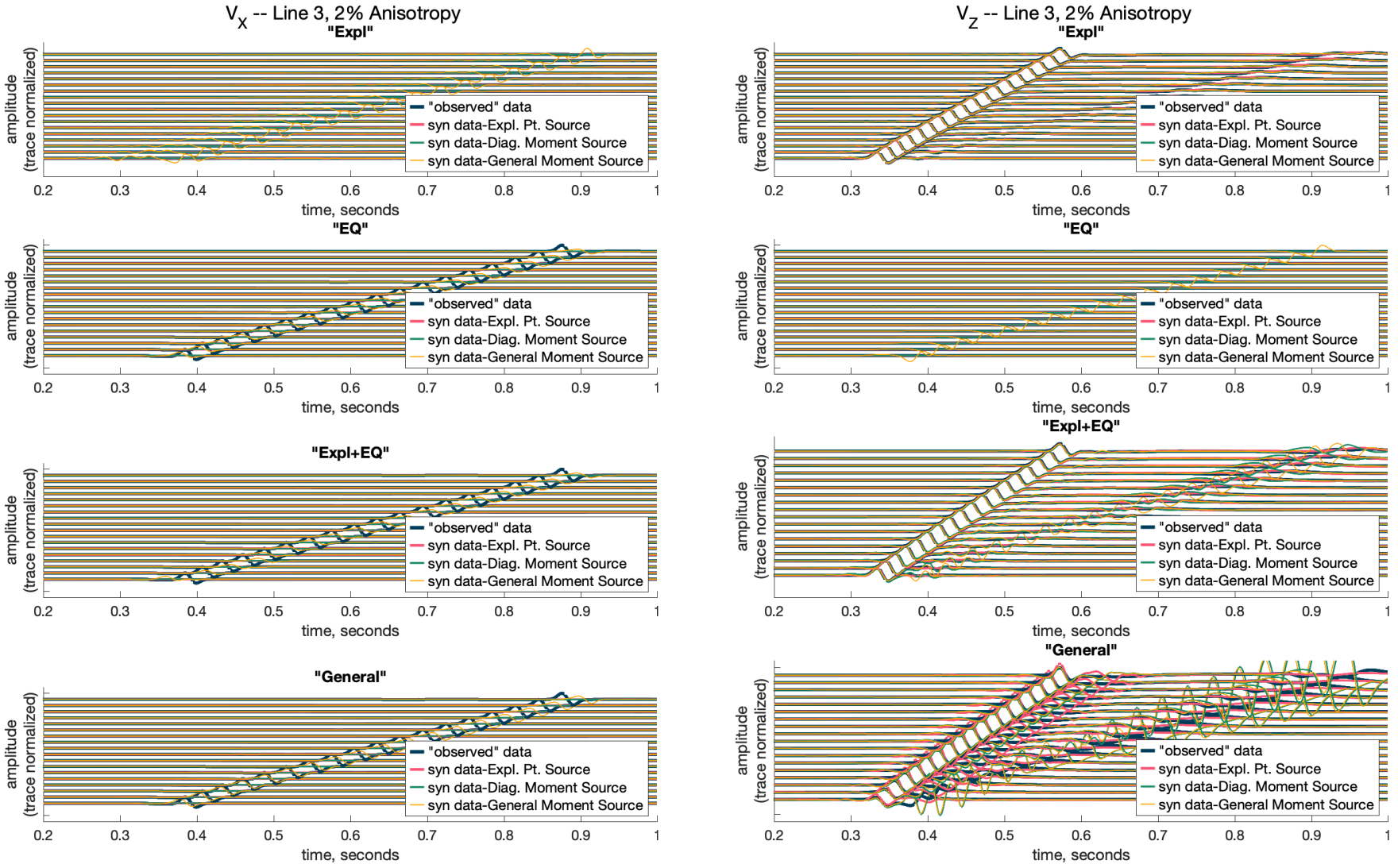

Figure A-13 V_X **and** V_Z **record sections of the isotropic GFs convolved with the estimated STF for Model Two, Case 2-2. The plots show the seismograms for all three source types used in generating the isotropic GFs (explosion, partial moment, and full moment source) with the seismograms for the 'observed' data. The plots labeled "Expl", "EQ", "Expl+EQ", and "General" correspond to the four different source types used to create the "observed" data (see Section 3.6.4). These seismograms are for receiver Line 3.**

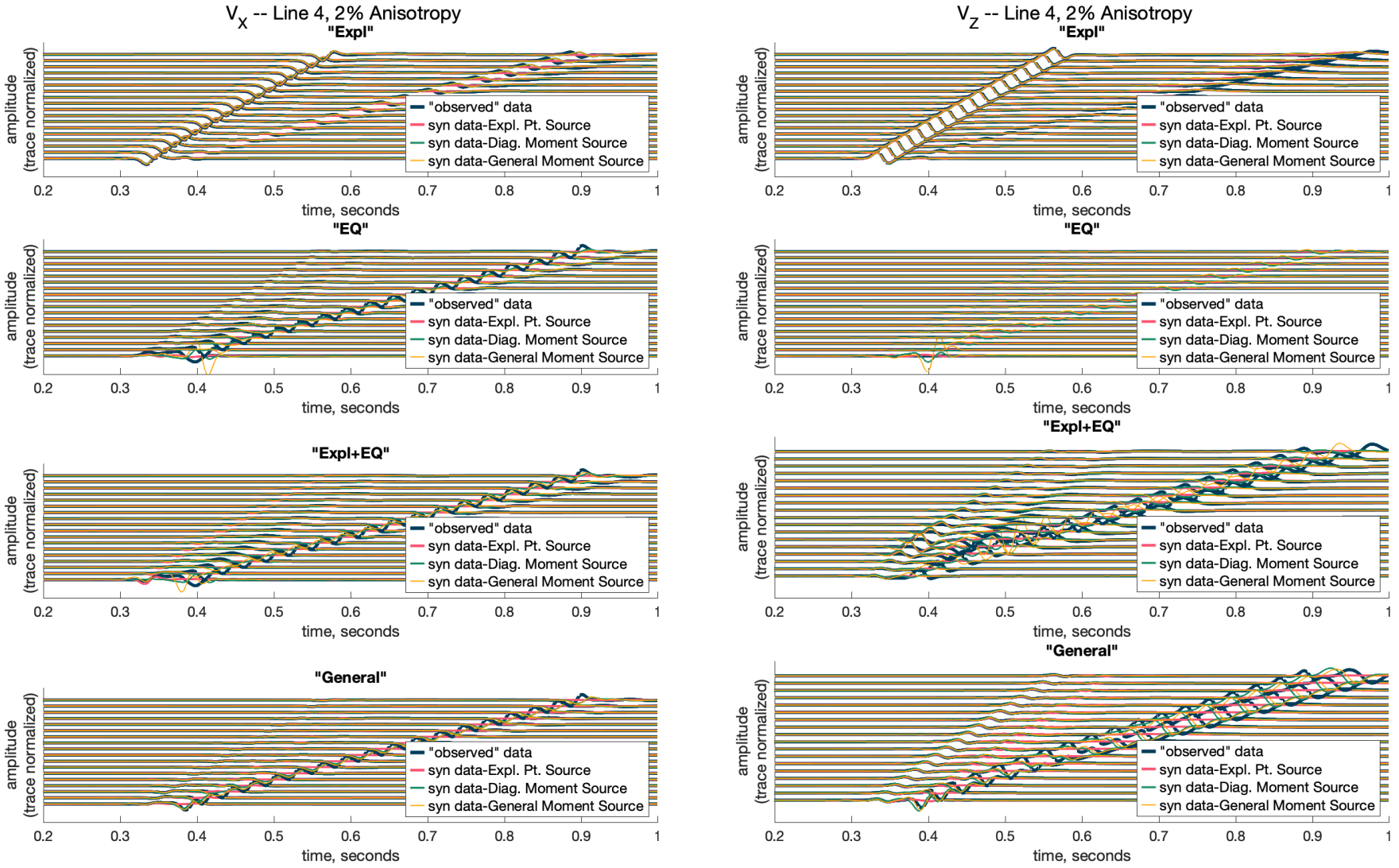

Figure A-14 V_X **and** V_Z **record sections of the isotropic GFs convolved with the estimated STF for Model Two, Case 2-2. The plots show the seismograms for all three source types used in generating the isotropic GFs (explosion, partial moment, and full moment source) with the seismograms for the 'observed' data. The plots labeled "Expl", "EQ", "Expl+EQ", and "General" correspond to the four different source types used to create the "observed" data (see Section 3.6.4). These seismograms are for receiver Line 4.**

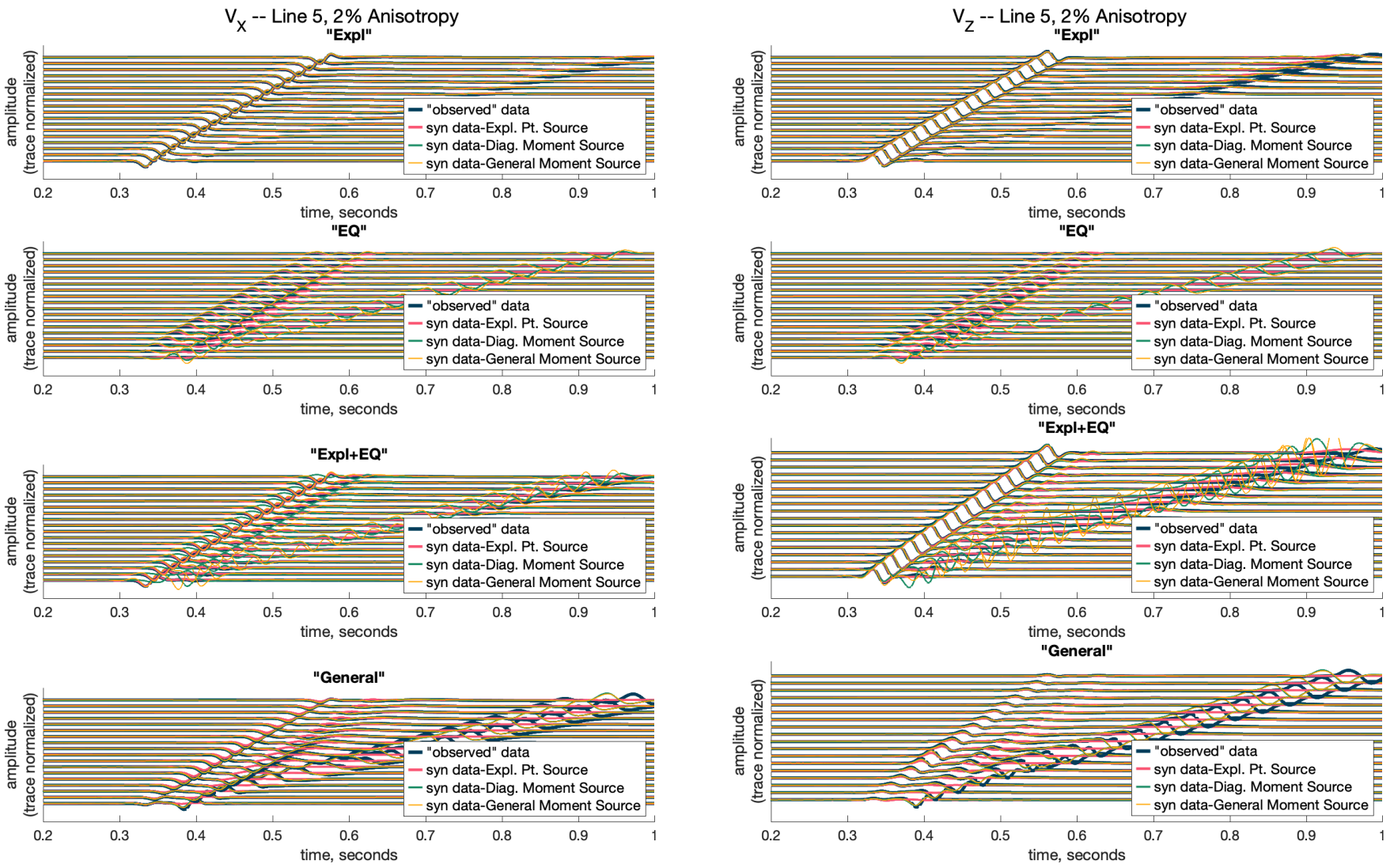

Figure A-15 V_X **and** V_Z **record sections of the isotropic GFs convolved with the estimated STF for Model Two, Case 2-2. The plots show the seismograms for all three source types used in generating the isotropic GFs (explosion, partial moment, and full moment source) with the seismograms for the 'observed' data. The plots labeled "Expl", "EQ", "Expl+EQ", and "General" correspond to the four different source types used to create the "observed" data (see Section 3.6.4). These seismograms are for receiver Line 5.**

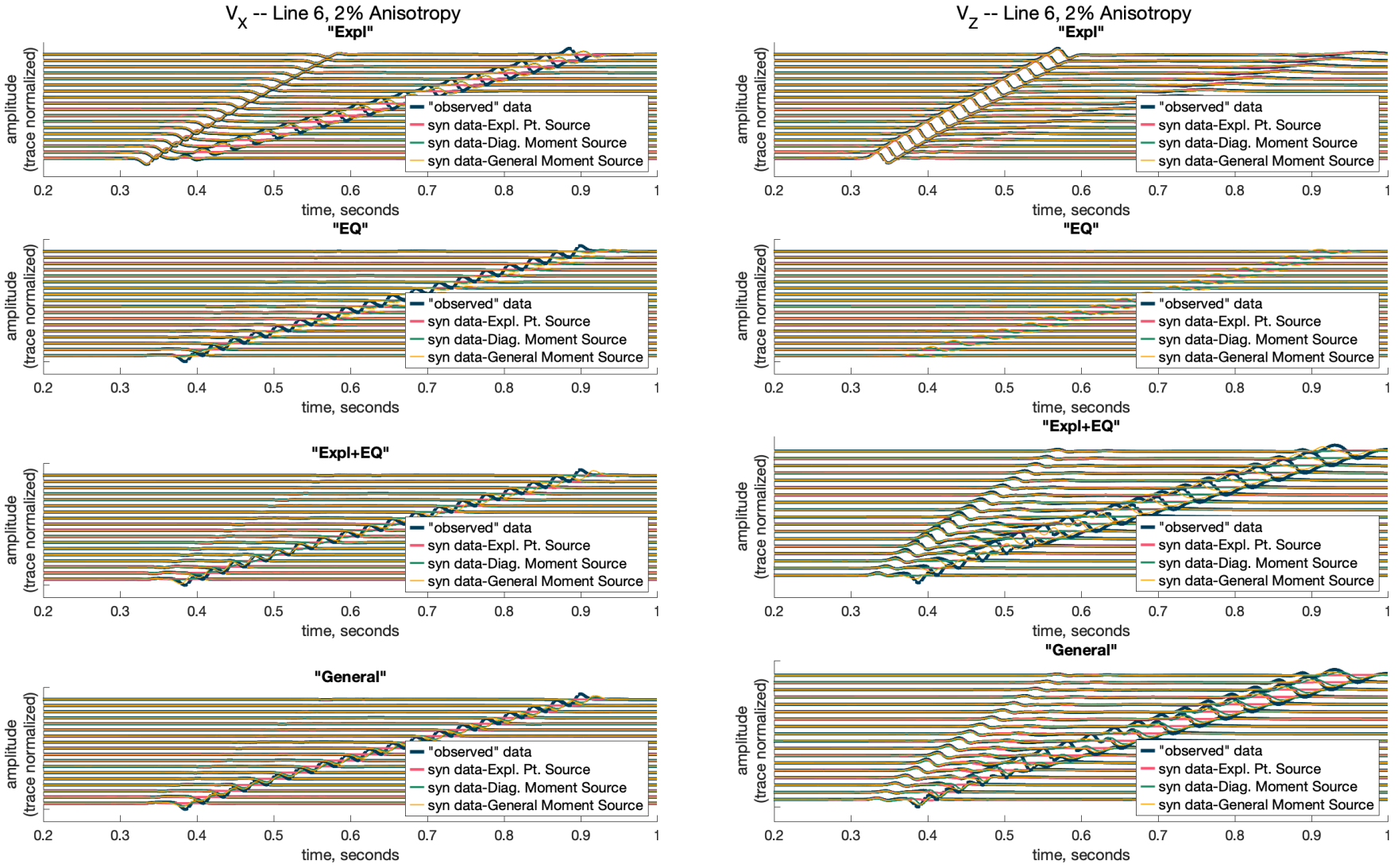

Figure A-16 V_X **and** V_Z **record sections of the isotropic GFs convolved with the estimated STF for Model Two, Case 2-2. The plots show the seismograms for all three source types used in generating the isotropic GFs (explosion, partial moment, and full moment source) with the seismograms for the 'observed' data. The plots labeled "Expl", "EQ", "Expl+EQ", and "General" correspond to the four different source types used to create the "observed" data (see Section 3.6.4). These seismograms are for receiver Line 6.**

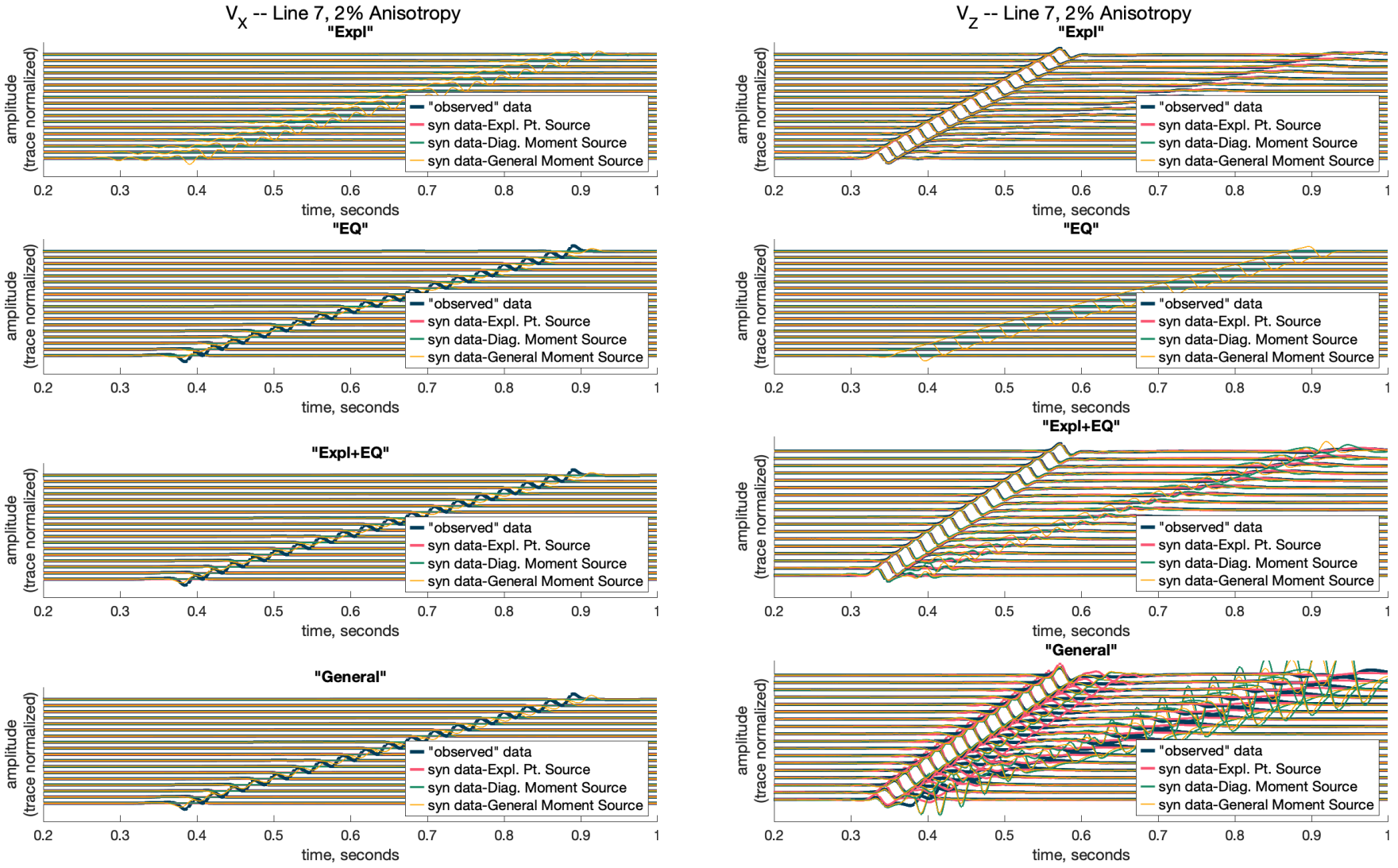

Figure A-17 V_X **and** V_Z **record sections of the isotropic GFs convolved with the estimated STF for Model Two, Case 2-2. The plots show the seismograms for all three source types used in generating the isotropic GFs (explosion, partial moment, and full moment source) with the seismograms for the 'observed' data. The plots labeled "Expl", "EQ", "Expl+EQ", and "General" correspond to the four different source types used to create the "observed" data (see Section 3.6.4). These seismograms are for receiver Line 7.**

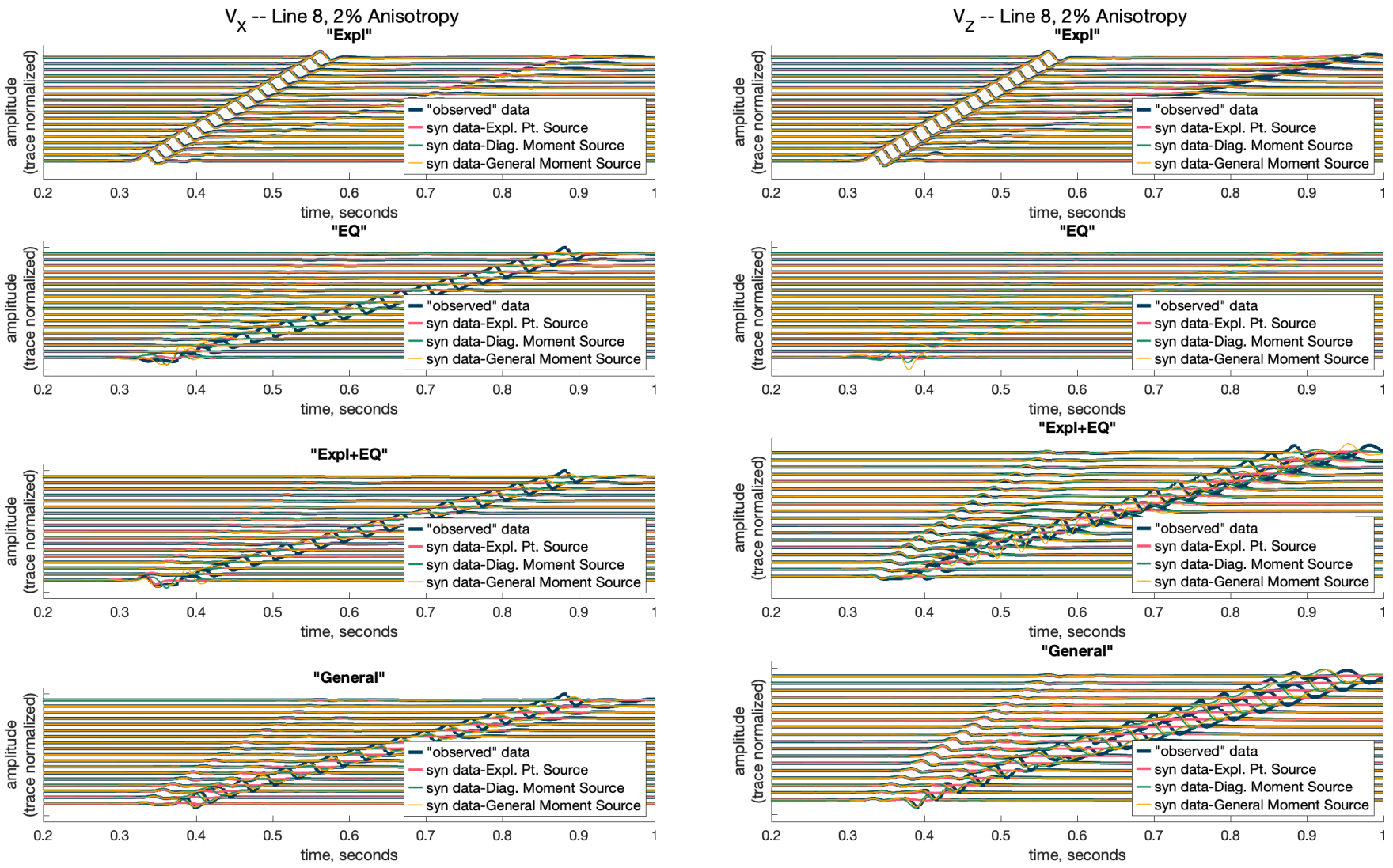

Figure A-18 V_X **and** V_Z **record sections of the isotropic GFs convolved with the estimated STF for Model Two, Case 2-2. The plots show the seismograms for all three source types used in generating the isotropic GFs (explosion, partial moment, and full moment source) with the seismograms for the 'observed' data. The plots labeled "Expl", "EQ", "Expl+EQ", and "General" correspond to the four different source types used to create the "observed" data (see Section 3.6.4). These seismograms are for receiver Line 8.**

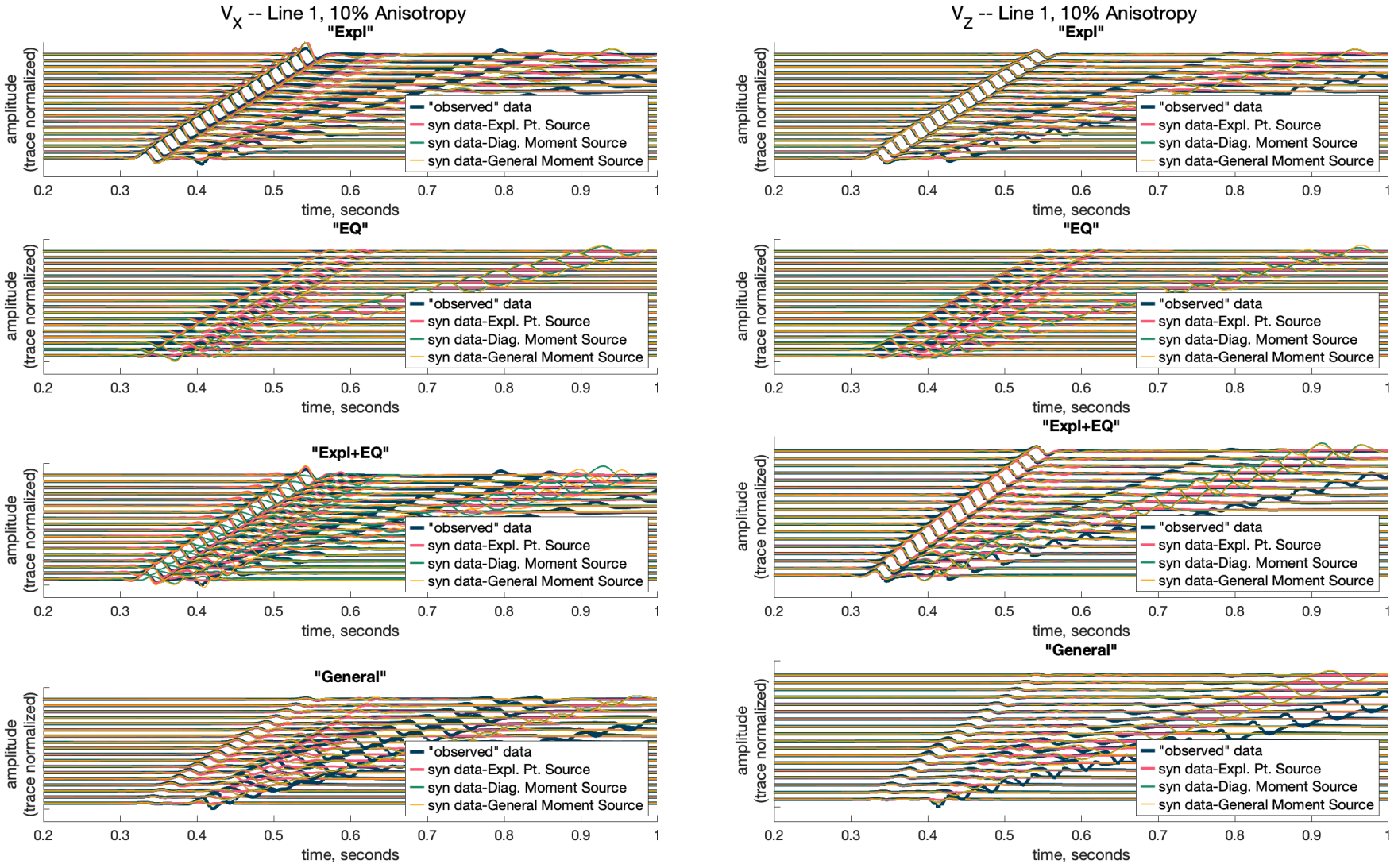

Figure A-19 V_X **and** V_Z **record sections of the isotropic GFs convolved with the estimated STF for Model Two, Case 2-3. The plots show the seismograms for all three source types used in generating the isotropic GFs (explosion, partial moment, and full moment source) with the seismograms for the 'observed' data. The plots labeled "Expl", "EQ", "Expl+EQ", and "General" correspond to the four different source types used to create the "observed" data (see Section 3.6.4). These seismograms are for receiver Line 1.**

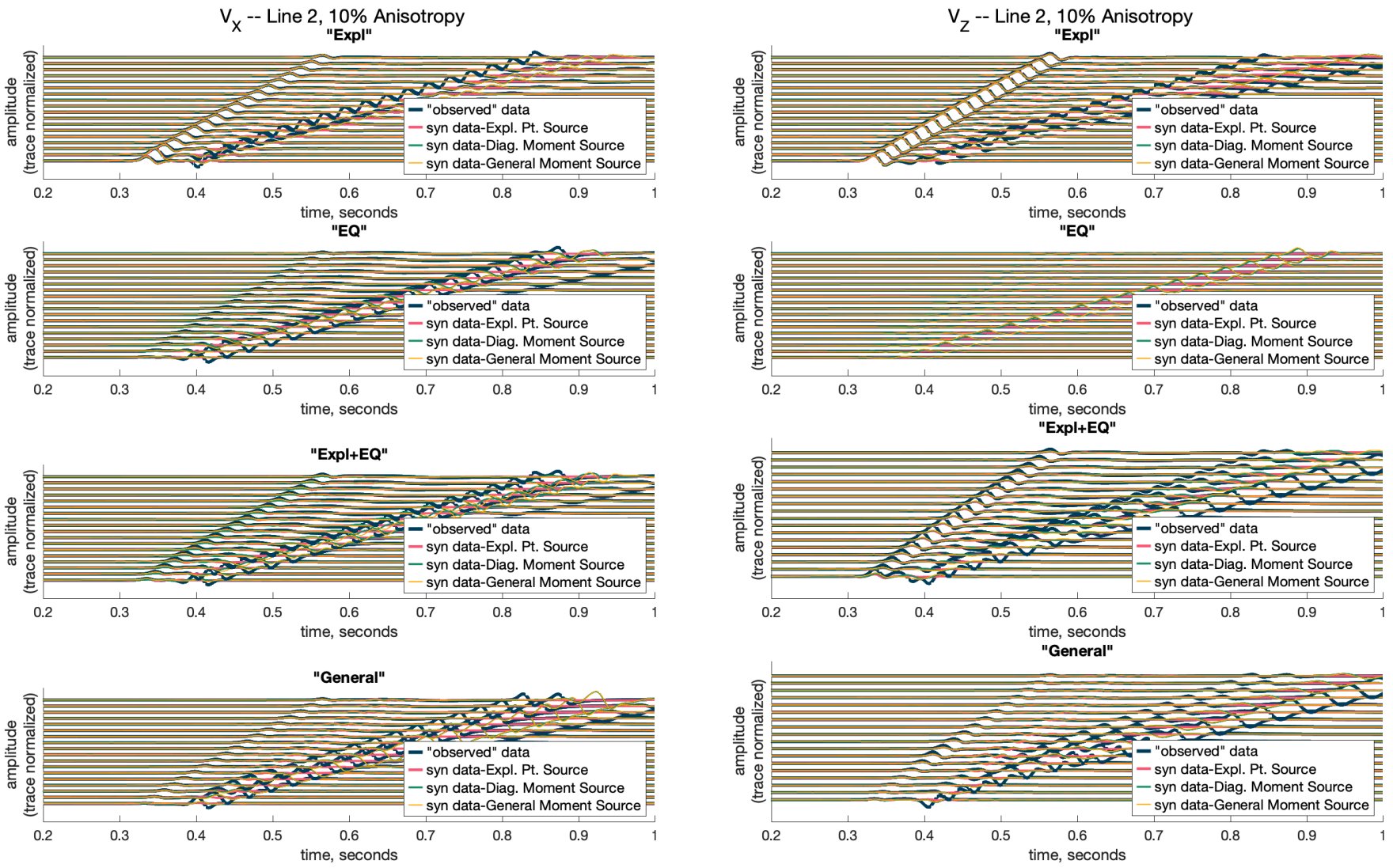

Figure A-20 V_X **and** V_Z **record sections of the isotropic GFs convolved with the estimated STF for Model Two, Case 2-3. The plots show the seismograms for all three source types used in generating the isotropic GFs (explosion, partial moment, and full moment source) with the seismograms for the 'observed' data. The plots labeled "Expl", "EQ", "Expl+EQ", and "General" correspond to the four different source types used to create the "observed" data (see Section 3.6.4). These seismograms are for receiver Line 2.**

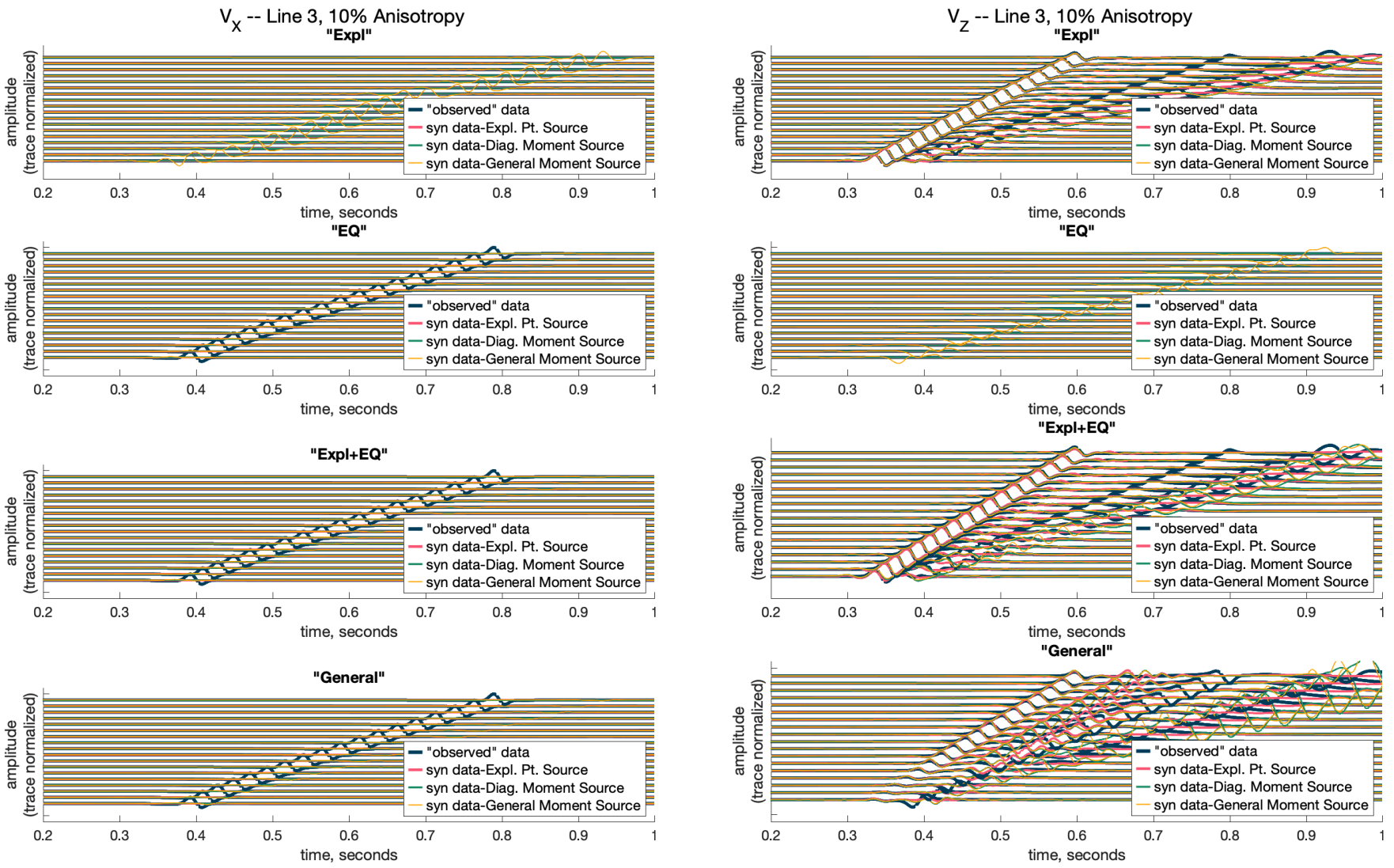

Figure A-21 V_X **and** V_Z **record sections of the isotropic GFs convolved with the estimated STF for Model Two, Case 2-3. The plots show the seismograms for all three source types used in generating the isotropic GFs (explosion, partial moment, and full moment source) with the seismograms for the 'observed' data. The plots labeled "Expl", "EQ", "Expl+EQ", and "General" correspond to the four different source types used to create the "observed" data (see Section 3.6.4). These seismograms are for receiver Line 3.**

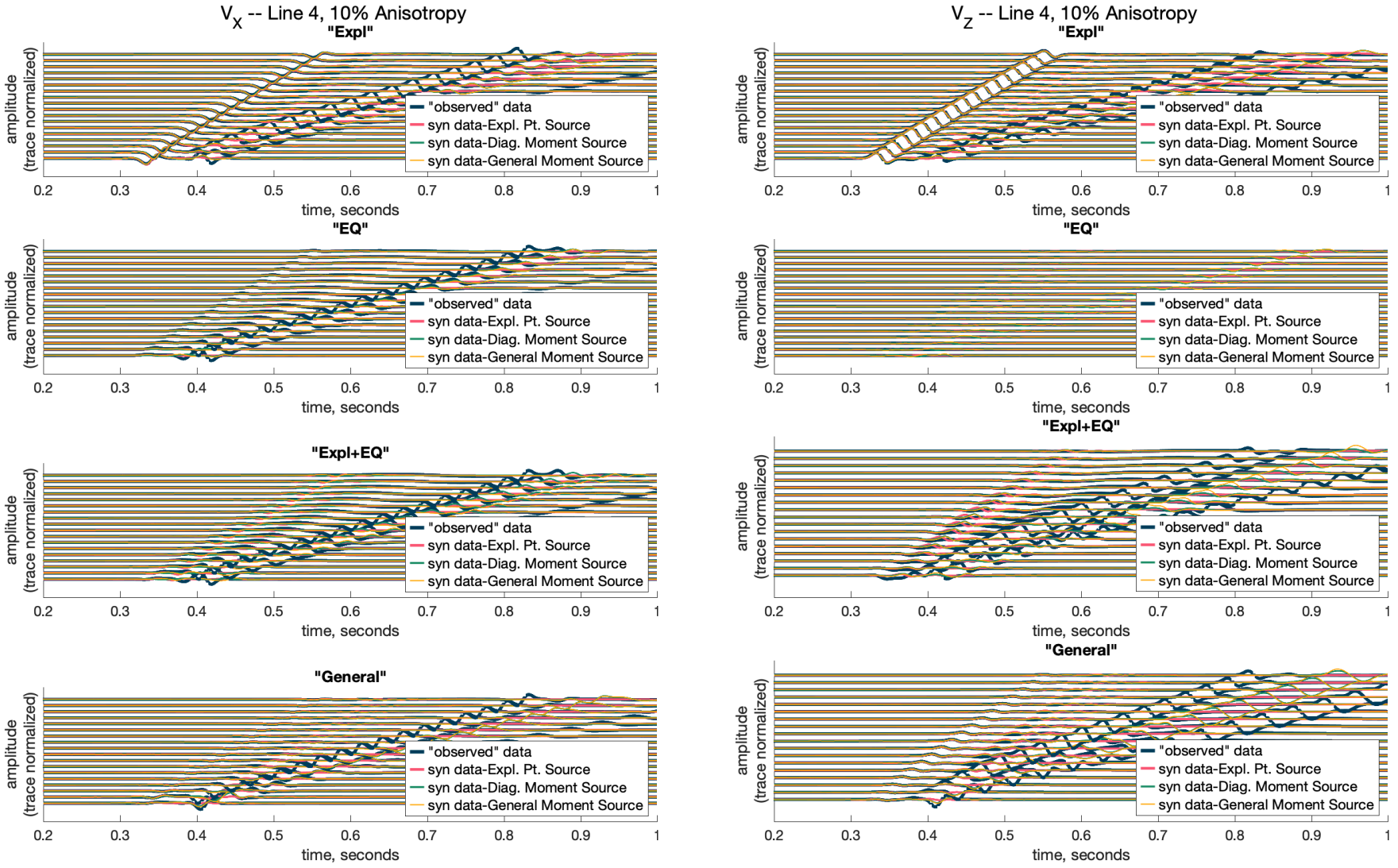

Figure A-22 V_X **and** V_Z **record sections of the isotropic GFs convolved with the estimated STF for Model Two, Case 2-3. The plots show the seismograms for all three source types used in generating the isotropic GFs (explosion, partial moment, and full moment source) with the seismograms for the 'observed' data. The plots labeled "Expl", "EQ", "Expl+EQ", and "General" correspond to the four different source types used to create the "observed" data (see Section 3.6.4). These seismograms are for receiver Line 4.**

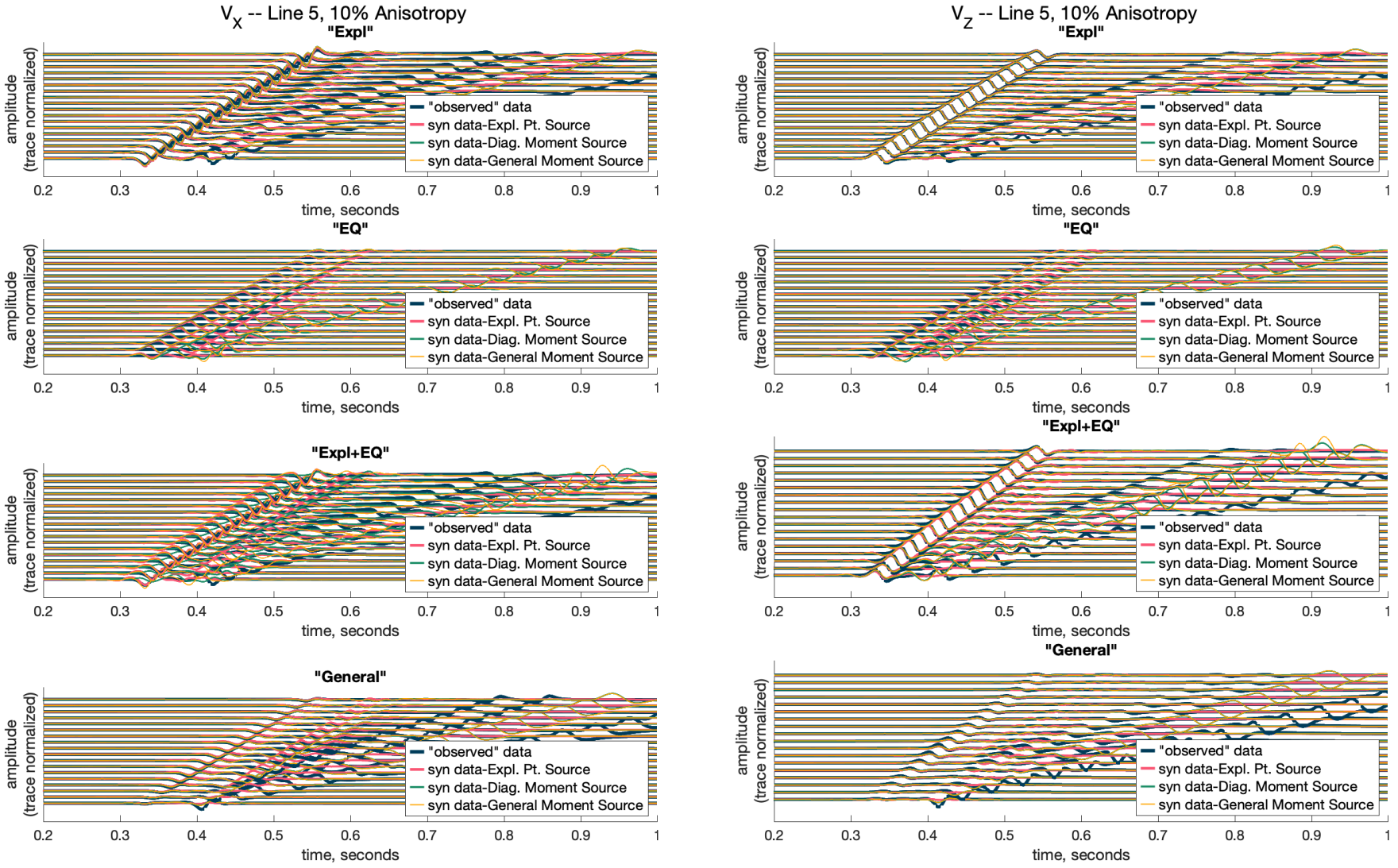

Figure A-23 V_X **and** V_Z **record sections of the isotropic GFs convolved with the estimated STF for Model Two, Case 2-3. The plots show the seismograms for all three source types used in generating the isotropic GFs (explosion, partial moment, and full moment source) with the seismograms for the 'observed' data. The plots labeled "Expl", "EQ", "Expl+EQ", and "General" correspond to the four different source types used to create the "observed" data (see Section 3.6.4). These seismograms are for receiver Line 5.**

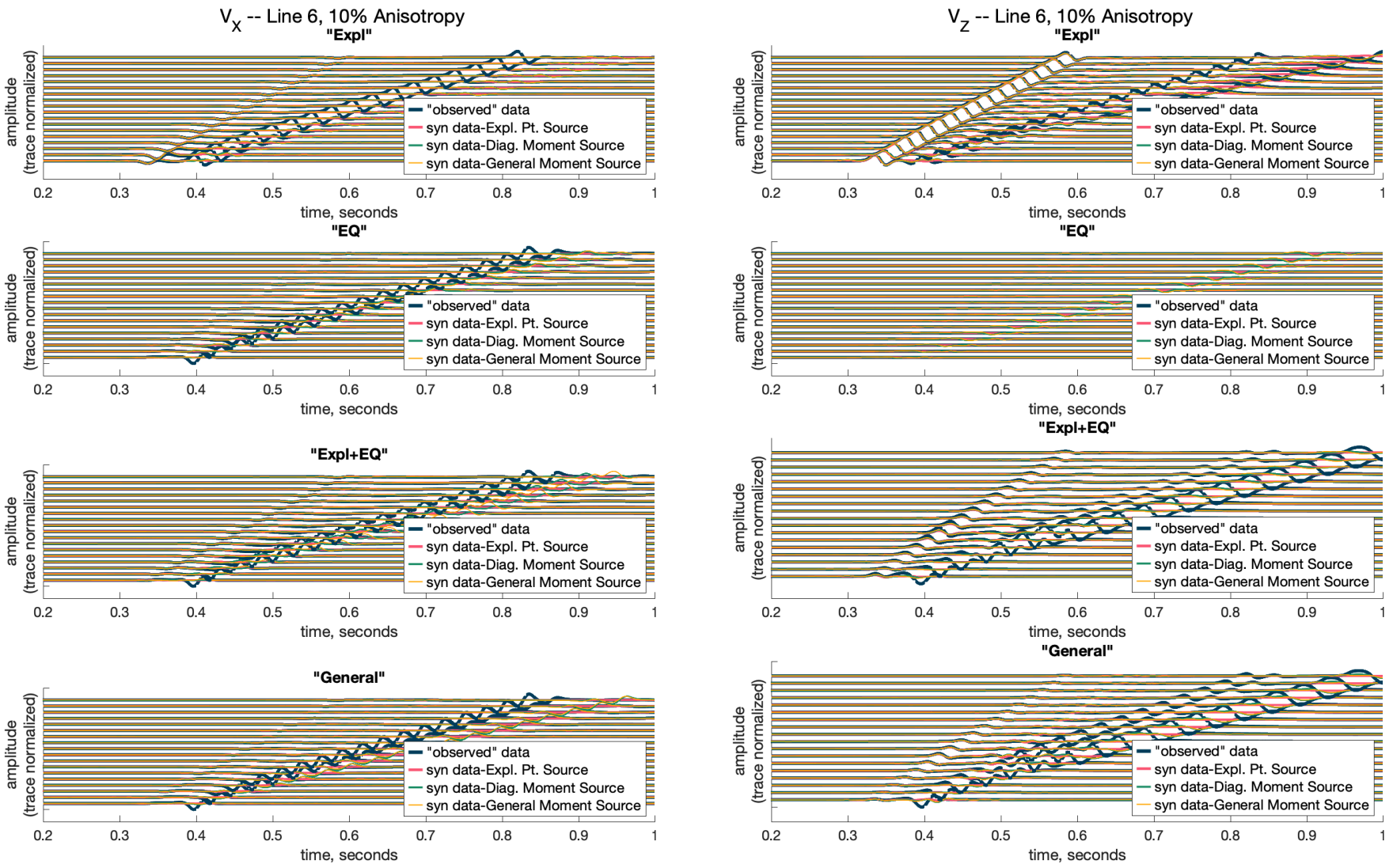

Figure A-24 V_X **and** V_Z **record sections of the isotropic GFs convolved with the estimated STF for Model Two, Case 2-3. The plots show the seismograms for all three source types used in generating the isotropic GFs (explosion, partial moment, and full moment source) with the seismograms for the 'observed' data. The plots labeled "Expl", "EQ", "Expl+EQ", and "General" correspond to the four different source types used to create the "observed" data (see Section 3.6.4). These seismograms are for receiver Line 6.**

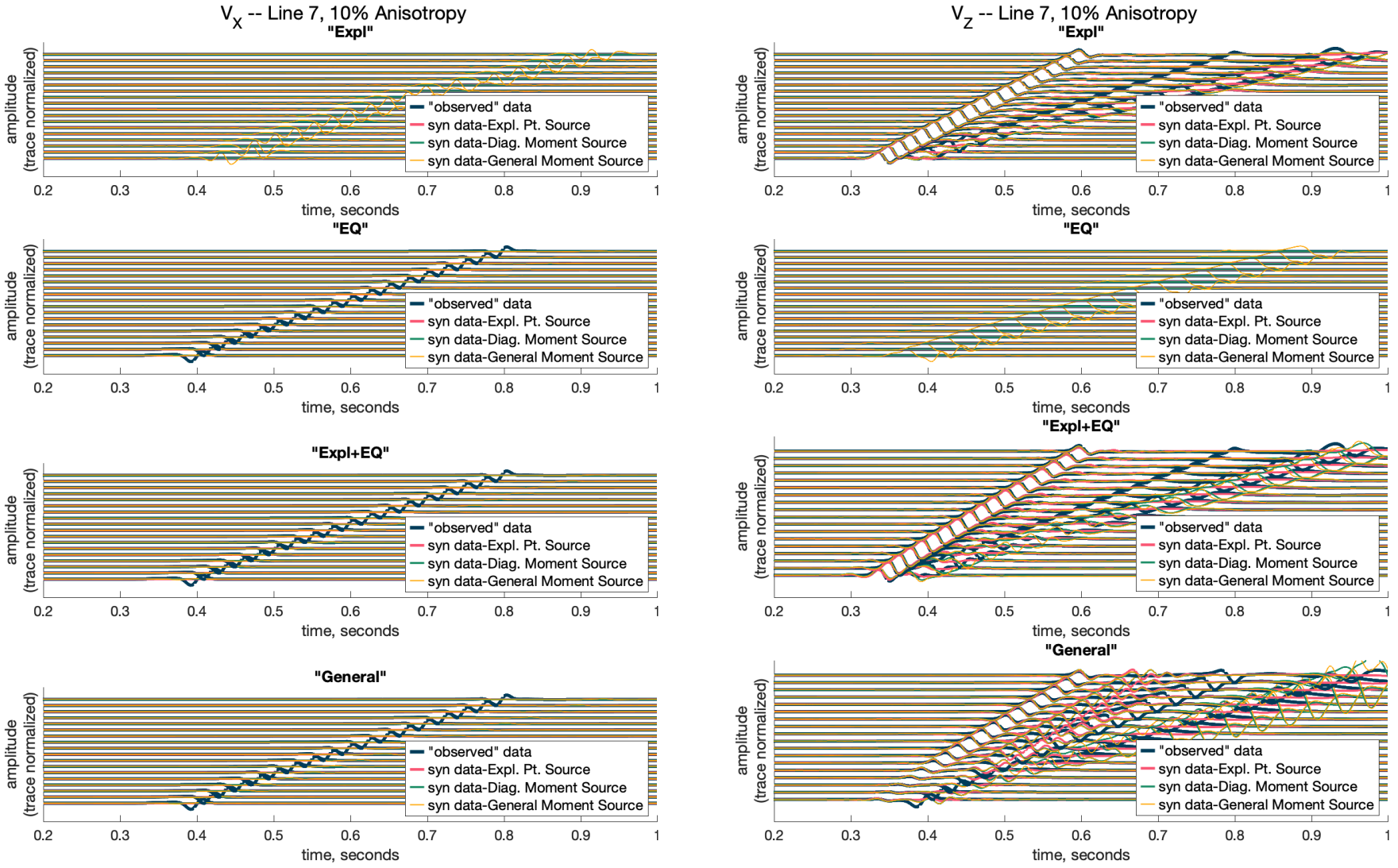

Figure A-25 V_X **and** V_Z **record sections of the isotropic GFs convolved with the estimated STF for Model Two, Case 2-3. The plots show the seismograms for all three source types used in generating the isotropic GFs (explosion, partial moment, and full moment source) with the seismograms for the 'observed' data. The plots labeled "Expl", "EQ", "Expl+EQ", and "General" correspond to the four different source types used to create the "observed" data (see Section 3.6.4). These seismograms are for receiver Line 7.**

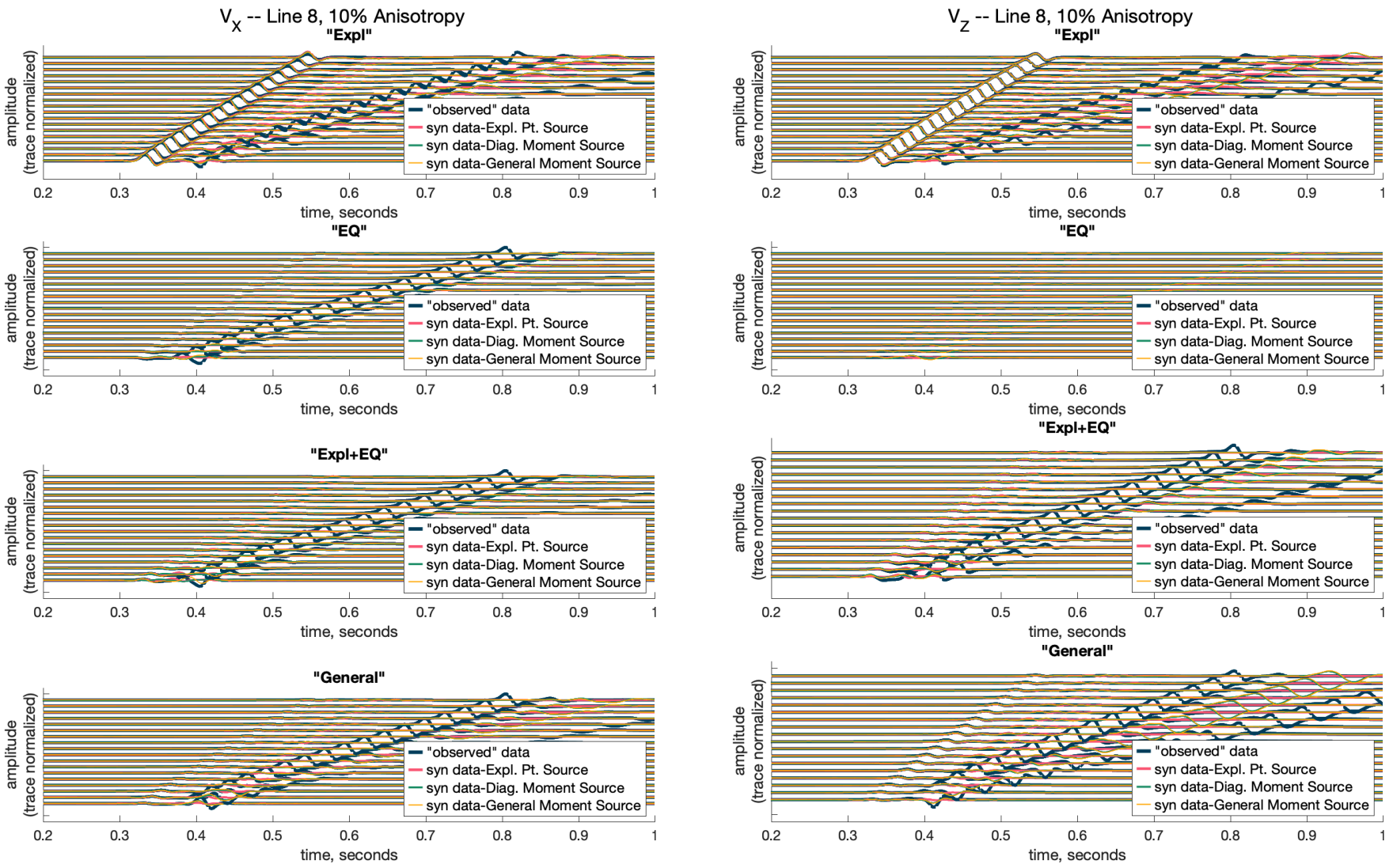

Figure A-26 V_X **and** V_Z **record sections of the isotropic GFs convolved with the estimated STF for Model Two, Case 2-3. The plots show the seismograms for all three source types used in generating the isotropic GFs (explosion, partial moment, and full moment source) with the seismograms for the 'observed' data. The plots labeled "Expl", "EQ", "Expl+EQ", and "General" correspond to the four different source types used to create the "observed" data (see Section 3.6.4). These seismograms are for receiver Line 8.**

DISTRIBUTION

Email—Internal [redacted]

Name	Org.	Sandia Email Address
Rob Abbott	08911	reabbot@sandia.gov
Kyle Jones	08911	krjones@sandia.gov
Leiph Preston	08911	lpresto@sandia.gov
Austin Holland	08914	aaholla@sandia.gov
Richard Jensen	08914	rpjense@sandia.gov
Technical Library	1911	sanddocs@sandia.gov

Sandia National Laboratories

Sandia National Laboratories is a multimission laboratory managed and operated by National Technology & Engineering Solutions of Sandia LLC, a wholly owned subsidiary of Honeywell International Inc., for the U.S. Department of Energy's National Nuclear Security Administration under contract DE-NA0003525.